

Original Article

Cite this article: Niu X, Dilek Y, Liu F, Feng G, and Yang J (2021) Early Devonian ultrapotassic magmatism in the North China Craton: geochemical and isotopic evidence for subcontinental lithospheric mantle metasomatism by subducted sediment-derived fluids. *Geological Magazine* **158**: 158–174. <https://doi.org/10.1017/S0016756819000797>

Received: 18 October 2018

Revised: 22 May 2019

Accepted: 30 May 2019

First published online: 6 August 2019

Keywords:

ultrapotassic plutonism; subcontinental lithospheric mantle metasomatism; Palaeo-Asian Ocean; Early Devonian tectonics; Central Asian Orogenic Belt; North China Craton; subducted sediment melting

Author for correspondence:

Xiaolu Niu, Email: niuxiaoludx@126.com

Early Devonian ultrapotassic magmatism in the North China Craton: geochemical and isotopic evidence for subcontinental lithospheric mantle metasomatism by subducted sediment-derived fluids

Xiaolu Niu¹ , Yildirim Dilek² , Fei Liu¹, Guangying Feng¹ and Jingsui Yang¹

¹Center for Advanced Research on Mantle (CARMA), Key Laboratory of Deep-Earth Dynamics of Ministry of Land and Resources, Institute of Geology, Chinese Academy of Geological Sciences, Beijing, 100037, China and ²Department of Geology & Environmental Earth Science, Miami University, Oxford, OH 45056, USA

Abstract

We report new U–Pb zircon age data, zircon *in situ* oxygen isotope, mineral chemistry, whole-rock geochemistry and Sr–Nd isotopic compositions from the Early Devonian ultrapotassic Gucheng pluton in the North China Craton, and discuss its petrogenesis. The Gucheng pluton is exposed in the northern part of the North China Craton and forms a composite intrusion, consisting of K-feldspar-bearing clinopyroxenite, clinopyroxene-bearing syenite and alkali-feldspar syenite. Mineral phases in these lithologies include clinopyroxene ($\text{Wo}_{43-48}\text{En}_{19-35}\text{Fs}_{18-38}$), sanidine ($\text{An}_0\text{Ab}_{3-11}\text{Or}_{89-97}$), and subordinate titanite, andradite and Na-feldspar. These rocks show homogeneous Sr but variable Nd isotopic compositions, and have relatively high zircon *in situ* oxygen isotopes ($\delta^{18}\text{O} = 5.2\text{--}6.7$). The Gucheng plutonic rocks formed through fractional crystallization and accumulation from ultrapotassic magmas, which were originated from partial melting of metasomatic vein systems in the subcontinental lithospheric mantle of the North China Craton. These vein networks developed as a result of the reactions of fluids derived from subducted pelitic sediments on the downgoing Palaeo-Asian ocean floor with the enriched, subcontinental lithospheric mantle peridotites. Sensitive high-resolution ion microprobe (SHRIMP) U–Pb zircon dating has revealed a crystallization age of 415 Ma for the timing of the emplacement of the Gucheng pluton that marks the early stages of alkaline magmatism associated with the Andean-type continental margin evolution along the northern edge of the North China Craton facing the Palaeo-Asian Ocean.

1. Introduction

The northern part of the North China Craton experienced repeated episodes of alkaline magmatism during the Palaeozoic and Mesozoic that were also associated with significant mineralization and ore-forming processes (Yan *et al.* 1999; Niu *et al.* 2012, 2016, 2017; Yang *et al.* 2012; Zhang *et al.*, 2012; Chen *et al.* 2013). Ultrapotassic plutonic rocks in orogenic belts display high contents of K_2O , high $\text{K}_2\text{O}/\text{Na}_2\text{O}$ ratios and other incompatible elements (Foley *et al.* 1987; Dilek & Altunkaynak 2010), and commonly represent partial melting products of a subcontinental lithospheric mantle (e.g. Feldstein & Lange, 1999; Miller *et al.* 1999; Williams *et al.* 2004; Avanzinelli *et al.* 2009; Zhao *et al.* 2009), which was previously metasomatized and enriched by slab-derived components (e.g. Conticelli & Peccerillo, 1992; Conticelli *et al.* 2007, 2015; Prelević *et al.* 2008; Jamali *et al.*, 2010; Tommasini *et al.* 2011; Altunkaynak *et al.* 2012; Liu *et al.* 2015; Wang *et al.* 2017). In the northern part of the North China Craton, the earliest phase of alkaline magmatism occurred in discrete pulses in the Early and Middle Devonian (Zhang *et al.* 2010; Huang & Hou 2017; this study) whereas the next episode of alkaline magmatism took place in the early Mesozoic (mainly in the Late Triassic; Yan *et al.* 1999; Niu *et al.* 2012, 2016, 2017; Yang *et al.* 2012; Chen *et al.* 2013). Widespread alkaline intrusive complexes constitute an E–W-trending alkaline magmatic belt that is more than 1500 km long along the northern North China Craton (Fig. 1).

These discrete episodes of alkaline magmatism and the temporally associated extensional deformation in the North China Craton are widely interpreted as being a result of post-collisional tectonics, which might have involved asthenospheric melt input due to slab break-off or lithospheric delamination. Slab break-off or lithospheric delamination processes are invoked in the existing models for the required heat source to cause partial melting of the metasomatized subcontinental lithospheric mantle. However, in many cases, the regional geological and geophysical evidence for such slab break-off or delamination events is absent, and the geological record

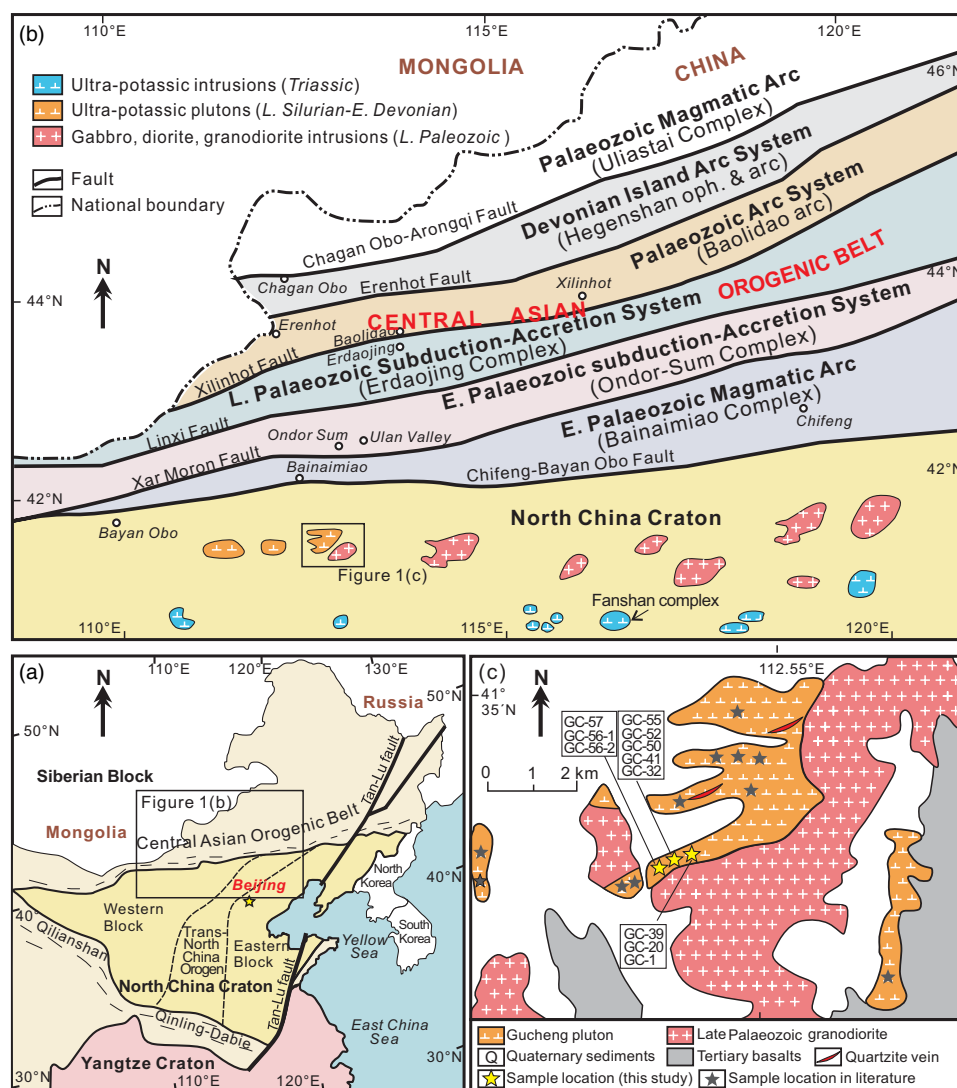


Fig. 1. (a) Simplified tectonic map of the North China Craton. (b) Simplified tectonics of the SE Central Asian Orogenic Belt (modified from Xiao *et al.* 2003). (c) Geological map of the Gucheng pluton.

indicates continued subduction of the Palaeo-Asian oceanic plate beneath the North China Craton throughout the middle to late Palaeozoic.

In this paper we address the mode and causes of alkaline magmatism in the northern part of the North China Craton through a case study of an Early Devonian ultrapotassic syenitic pluton (Gucheng pluton), and discuss its petrogenesis within the framework of the regional geology and tectonics. We first present new zircon U–Pb dating results and detailed mineral, whole-rock chemistry, and Sr–Nd and zircon *in situ* oxygen isotope data from this pluton. We then evaluate the nature of its parental magmas, and its melt evolution and the characteristics of its mantle source through a new chemical geodynamics model. Our proposed tectonomagmatic model differs from the existing ones in regard to the potential causes and mechanisms of the enrichment and partial melting of the subcontinental lithospheric mantle beneath the North China Craton.

2. Regional geology of the North China Craton

The North China Craton represents one of the oldest and largest cratons on Earth with a nearly complete record of Precambrian

history (Jahn *et al.* 1987; Liu *et al.* 1992). The Proterozoic–Palaeozoic Central Asian Orogenic Belt (also known as the Altaiids) to the north is a major accretionary-type orogen (Fig. 1a). The Qilianshan, Qinling–Dabie orogenic belts and the Tan–Lu fault delimit the North China Craton to the west, south and east, respectively. The North China Craton itself is divided into the Western and Eastern Blocks by the 100- to 300-km-wide, NNE–SSW-trending Trans-North China Orogen (Fig. 1a; Zhao 2001).

The Eastern Block consists of early to late Archaean tonalite–trondhjemite–granodiorite and granitic gneiss terranes that are tectonically integrated with felsic to ultramafic greenstones (meta-volcanic and meta-sedimentary rocks) (Zhao & Zhai, 2013; Wei *et al.* 2014). These Archaean basement units are overlain by Proterozoic rift basin strata and variously metamorphosed sedimentary and volcanic rock sequences. The Eastern Block underwent successive episodes of rifting, magmatism and strike-slip faulting in the upper plate of the Palaeo-Pacific subduction zone, dipping obliquely beneath East Asia during the Late Triassic through the Jurassic–Cretaceous (Wang *et al.* 2018). These Mesozoic events resulted in significant thinning and destabilization of the North China Craton in the east (Wu *et al.* 2005; Zhu *et al.* 2012).

The Western Block consists mainly of a Neoproterozoic (2.6–2.5 Ga) basement composed of tonalite–trondhjemite–granodiorite and meta- mafic and meta-sedimentary rocks. Palaeoproterozoic meta-pelitic rocks overlie these Archaean basement lithologies and are in turn overlain by undeformed Phanerozoic sedimentary sequences.

The Central Asian Orogenic Belt to the north of the North China Craton developed through successive episodes of subduction–accretion events, punctuated by the collapse of fringing island arc systems, which evolved within the Palaeo-Asian Ocean (Windley *et al.* 2007). The Ordovician – Early Devonian Bainaimiao plutonic–volcanic complexes in the northern North China Craton represent an Andean-type magmatic arc system, developed above a Palaeo-Asian Ocean slab dipping southwards beneath the North China Craton (Xiao *et al.* 2003; Song *et al.* 2015, and references therein). This magmatic arc complex includes calc-alkaline plutons composed of granite, granodiorite, tonalite, quartz diorite and hornblende gabbro, and volcanic sequences composed of tholeiitic basalt, alkaline basalt, andesite, rhyolite, agglomerate and tuffaceous rocks that are intercalated with chert, sandstone and conglomerate; high initial Sr isotope ratios (0.7146) and ϵ_{Nd} values ($+2.4 \pm 1.7$) obtained from granitic and granodioritic rocks of the Bainaimiao arc complex suggest the involvement of Proterozoic and older crustal basement rocks in the melt evolution of arc magmas (Zhang *et al.* 2014, and references therein). All these plutonic, volcanic and sedimentary rocks of the Bainaimiao arc are affected by N-directed thrust faults, consistent with the geometry of the S-dipping Palaeo-Asian Ocean slab. Zircon U–Pb ages available from the Bainaimiao plutonic and dyke rocks range from 472 Ma to 411 ± 8 Ma, and the volcanic rocks from 474 ± 5 Ma to 436 ± 9 Ma (Zhang *et al.* 2014). These ages indicate that the Bainaimiao ensialic arc magmatism occurred during the Early–Middle Ordovician through Early Devonian.

An Early Ordovician (490–470 Ma) subduction–accretion complex and ophiolitic rock sequences with mid-ocean ridge basalt (MORB), island arc tholeiitic and boninitic geochemical affinities that are characteristic of fore-arc oceanic crust (Dilek & Furnes, 2011, 2014) occur north of the Bainaimiao magmatic arc (Xiao *et al.* 2003; Wilhem *et al.* 2012). These ophiolitic and accretionary prism rocks are emplaced southwards onto the North China Craton and are interpreted to represent an Early Ordovician island arc complex (Ulan island arc of Xiao *et al.* 2003), which was developed above a N-dipping subduction zone within the Palaeo-Asian Ocean. The collision of the northern passive margin of the North China Craton with this island arc system took place in the early Ordovician and resulted in the accretion of the Ulan island arc to the North China Craton prior to 470 Ma (Xiao *et al.* 2003; Wilhem *et al.* 2012).

This arc–continent collision was followed by the initiation of a new subduction zone dipping southwards that resulted in the establishment of a long-lived Andean-type active continental margin along the northern edge of the North China Craton. The Ondor–Sum accretionary complex, with blueschist rocks ranging in age from 446 to 426 Ma (Xiao *et al.* 2003), and the Middle Ordovician – Early Devonian Bainaimiao ensialic arc formed at this active margin; steepening slab geometry keeping pace with the slab rollback at this S-dipping subduction zone caused the Bainaimiao arc magmatism to migrate northwards through time (Wilhem *et al.* 2012; Song *et al.* 2015). Both the Bainaimiao magmatic arc rocks and the Ondor–Sum accretionary complex are unconformably overlain by Early–Middle Devonian shallow marine clastic rocks, suggesting that the Andean-type continental

margin magmatism was no longer active by 400 Ma (Wilhem *et al.* 2012, and references therein).

A renewed episode of large-scale intracontinental magmatism in the northern part of the North China Craton started nearly 40 million years later, *c.* 360 Ma, and lasted until 258 Ma, mainly represented by calc-alkaline, high-K calc-alkaline plutons to the south of the Bainaimiao continental arc (Zhang *et al.* 2012; Song *et al.* 2015).

The timing of the complete amalgamation of the Siberian Block and the North China Craton has been constrained to a period from *c.* 270 to 250 Ma (Chen *et al.* 2009; Zhang *et al.* 2009). During the Late Triassic, this continental collision zone and the northern margin of the North China Craton experienced extensive ultrapotassic, alkaline magmatism in an ~E–W-trending, orogen-parallel belt (represented by the Fanshan ultramafic–syenitic complex; Fig. 1b) (Yan *et al.* 1999; Niu *et al.* 2012, 2016, 2017; Yang *et al.* 2012; Chen *et al.* 2013; Hou *et al.* 2015). These ultrapotassic and alkaline igneous complexes share some common features in their whole-rock and mineral compositions: (i) they are dominantly composed of clinopyroxene/biotite-bearing syenite, alkali-feldspar syenite and/or ultramafic rocks (clinopyroxenite, glimmerite, biotite-bearing clinopyroxenites, K-feldspar-bearing clinopyroxenite); and (ii) clinopyroxene, K-feldspar, biotite, and/or melanite, and/or nepheline, are the main constituent minerals; these intrusive rocks are free in olivine.

3. Field occurrence and mineralogy of the Gucheng pluton

The Gucheng pluton is part of a series of ~E–W-trending small intrusive bodies near the Chifeng–Bayan Obo fault zone along the northern edge of the North China Craton (Fig. 1a, b). It crops out in a ~20 km² sub-circular exposure, intruded in the east and the south by a Carboniferous granitoid pluton and pegmatites, and covered on all sides by Cenozoic flood basalts and Quaternary alluvial sediments (Fig. 1c). Also known as the Sandaogou intrusive complex (XH Zhang *et al.* 2010; QQ Zhang *et al.* 2018), the Gucheng pluton consists of magmatic bands of K-feldspar-bearing clinopyroxenite, clinopyroxene-bearing syenite and alkali-feldspar syenite (Fig. 2a). The K-feldspar-bearing clinopyroxenite and the clinopyroxene-bearing syenite have gradational contacts and form well-developed layers marked by clinopyroxene and K-feldspar-rich bands (Fig. 2a). These two lithologies are cross-cut by veins and dikelets of alkali-feldspar syenite whose orientations and geometries are controlled by brittle fracture networks (Fig. 2a). These outcrop features suggest that the injection of alkali-feldspar melt into the Gucheng pluton took place after the cooling and solidification of the other two magma types. All three alkaline rock types are cut and displaced by high-angle normal faults as a result of N–S extension (Fig. 2a).

The K-feldspar-bearing clinopyroxenite is composed of coarse-grained, accumulate euhedral clinopyroxene (>80 %), interstitial sanidine (5–15 %), euhedral titanite (2–8 %) and minor garnet (1–5 %) (Fig. 2b). The clinopyroxene-bearing syenite consists mainly of varying proportions of subhedral to euhedral clinopyroxene (5–20 %), coarse-grained K-feldspar (60–80 %) and accessory titanite (2–8 %) (Fig. 2c). The alkali-feldspar syenite comprises coarse-grained K-feldspar (>95 %) and minor garnet (<3 %) (Fig. 2d).

4. Sample selection

Previous studies have mainly focused on the clinopyroxene-bearing syenite unit sampled in the central and northern parts of the pluton

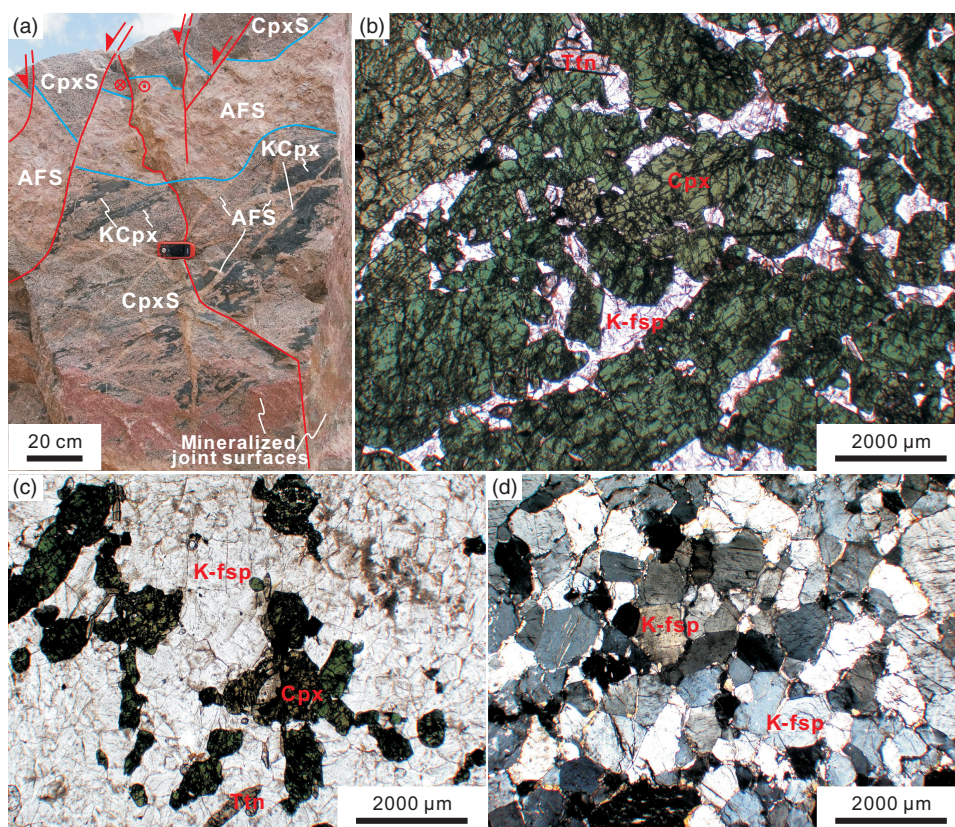


Fig. 2. (a) Outcrop image of the Gucheng pluton, showing the contact relationships between the main lithologies and the extensional normal fault patterns. (b–d) Photomicrographs of K-feldspar-bearing clinopyroxenite (plain-polarized light), clinopyroxene-bearing syenite (plain-polarized light) and alkali-feldspar syenite (crossed polars), respectively. AFS = alkali-feldspar syenite; CpxS = clinopyroxene-bearing syenite; KCpx = K-feldspar-bearing clinopyroxenite; K-fsp, K-feldspar; Cpx, clinopyroxene; Ttn, titanite.

(Fig. 1c; XH Zhang *et al.* 2010; QQ Zhang *et al.* 2018). In this study, we have identified a large outcrop in an abandoned quarry within the southern part of the pluton, where K-feldspar-bearing clinopyroxenite, clinopyroxene-bearing syenite, and alkali-feldspar syenite occur together. We sampled these three lithological units for our investigations. See Figure 1c for the location of the samples, and Supplementary File 1 in the online Supplementary Material at <https://doi.org/10.1017/S0016756819000797> for their GPS geographical coordinates.

K-feldspar-bearing clinopyroxenite rocks (samples GC-57, GC-56-1 and GC-56-2) occur as discrete layers and lenses in the outcrop. They are composed of coarse-grained, accumulate euhedral clinopyroxene (>80%), interstitial sanidine (5–15%), euhedral titanite (2–8%) and minor garnet (1–5%) (Fig. 2b). This K-feldspar-bearing clinopyroxenite unit has never been reported from the Gucheng pluton in previous studies.

Clinopyroxene-bearing syenite rocks (samples GC-55, GC-52, GC-50, GC-41 and GC-32) are the most common lithological unit in the Gucheng pluton. They consist mainly of varying proportions of subhedral to euhedral clinopyroxene (5–20%), coarse-grained K-feldspar (60–80%), and accessory titanite (2–8%) (Fig. 2c).

Alkali-feldspar syenite rocks (samples GC-39, GC-20 and GC-1) comprise coarse-grained K-feldspar (>95%) and minor garnet (<3%) (Fig. 2d).

Previous studies reported the elemental compositions of clinopyroxene-bearing syenites and their U–Pb zircon ages (XH Zhang *et al.* 2010; QQ Zhang *et al.* 2018). In this study, we analysed the elemental (major, trace and Sr–Nd isotopes) compositions of the newly discovered K-feldspar-bearing clinopyroxenite and alkali-feldspar syenite units within the pluton. In addition, we chose an alkali-feldspar syenite sample (GC-1) for zircon U–Pb

dating and oxygen isotope analysis, for it was difficult to separate zircons from clinopyroxenites. We also analysed the elemental compositions of our clinopyroxene-bearing syenite samples for comparison with the published data.

5. Analytical methods

5.a. Whole-rock major and trace element analyses

Whole-rock major and trace element measurements were performed at National Research Center of Geoanalysis, Beijing, China. Major elements were determined by X-ray fluorescence, using fused glass discs with analytical uncertainty <1%. Trace elements were measured using inductively coupled plasma mass spectrometry (ICP-MS). Analytical uncertainties are 10% for elements with abundances <10 ppm and *c.* 5% for those >10 ppm. The standard sample GBW07109 was prepared and analysed with the same analytical procedure as the samples (repetition *n* = 1). The measured and recommended values of major and trace element composition of the standard sample GBW07109 are listed in Supplementary File 2 (online Supplementary Material at <https://doi.org/10.1017/S0016756819000797>).

5.b. Mineral chemistry analyses

Major elements of clinopyroxene, feldspar, titanite and garnet were measured on a JXA-8100 electron microprobe at the Key Laboratory of Deep-Earth Dynamics of Ministry of Land and Resources in the Institute of Geology at the Chinese Academy of Geological Sciences, Beijing (China), using an accelerating voltage of 15 kV, beam current of 10 nA and spot diameter of 1 μm. We used the PRZ method for corrections. We utilized standard

samples (53 kinds of minerals produced by US SPI Company) throughout the analytical work. Our reported precision was better than 1 %.

5.c. SHRIMP U–Pb zircon dating and zircon *in situ* oxygen isotope analysis

Zircon grains were extracted by heavy-liquid and magnetic methods, and were further purified by hand-picking under a binocular microscope. Zircons were mounted onto an epoxy resin disc together with several grains of standard zircon TEMORA, and were then polished to examine their interiors. Photomicrographs and cathodoluminescence images were taken to examine their internal structures and to select the optimum positions for analysis.

Zircon U–Th–Pb analyses were performed using the SHRIMP II (sensitive high-resolution ion microprobe) instrument at Beijing SHRIMP Center in the Institute of Geology at the Chinese Academy of Geological Sciences in Beijing (China). Spot diameter was 30 μm . Detailed analytical procedures of Williams (1998) were followed. Data were processed and assessed using the SQUID1.0 and ISOPLOT software of Ludwig (2001, 2003). Measured ^{204}Pb was used to for common Pb correction. The separated zircon grains were polished and cleaned thoroughly in order to eliminate any possible contamination prior to the *in situ* oxygen isotope analyses. SHRIMP II instrument at Beijing SHRIMP Center, following the analytical procedures of Ickert *et al.* (2008). We report the oxygen isotopic data here by $\delta^{18}\text{O}$ values with reference to the Vienna Standard Mean Ocean Water (V-SMOW) standard.

5.d. Whole-rock Sr–Nd isotope analyses

Separation and purification of Sr and Nd were done through conventional cation exchange procedures at the Key Laboratory of Orogenic Belts and Crustal Evolution in Peking University of Beijing (China). Sr and Nd isotopic compositions were measured in a negative ion detection mode on a Thermo-Finnigan TRITON[®] mass spectrometer at Tianjin Institute of Geology and Mineral Resources, Tianjin (China). Detailed analytical procedures and experimental conditions are given in Niu *et al.* (2017). During the period of data acquisition, Jndi-1 Nd standard yielded $^{143}\text{Nd}/^{144}\text{Nd} = 0.512104 \pm 0.000003$ (2σ) (repetition $n = 1$), and Sr standard NBS-987 gave $^{87}\text{Sr}/^{86}\text{Sr} = 0.710264 \pm 0.000004$ (2σ) (repetition $n = 1$). The BCR-2 standard, prepared with the same analysis procedure as the samples, yielded $^{143}\text{Nd}/^{144}\text{Nd} = 0.512626 \pm 0.000006$ (2σ), and $^{87}\text{Sr}/^{86}\text{Sr} = 0.705075 \pm 0.000008$ (2σ) (repetition $n = 1$).

6. Results

6.a. Whole-rock major and trace element compositions

We present the major and trace element contents of the analysed rocks from the Gucheng pluton in Table 1.

The analysed rocks show variable major element compositions, with $\text{SiO}_2 = 50.89\text{--}65.11$ wt %, $\text{Al}_2\text{O}_3 = 3.87\text{--}18.39$ wt %, Fe_2O_3 total = $0.23\text{--}15.26$ wt %, $\text{MgO} = 0.05\text{--}7.18$ wt %, $\text{CaO} = 0.08\text{--}16.2$ wt %, $\text{Na}_2\text{O} = 1.31\text{--}2.02$ wt % and $\text{K}_2\text{O} = 2.03\text{--}13.38$ wt %. As seen in the plots of major element variations against SiO_2 (Fig. 3), with increasing SiO_2 values, the Al_2O_3 , K_2O and $\text{Na}_2\text{O} + \text{K}_2\text{O}$ contents increase, whereas CaO , MgO , Fe_2O_3 , P_2O_5 and TiO_2 decrease significantly. These compositional variations are mainly due to the varying proportions of clinopyroxene, K-feldspar, titanite and

garnet in the analysed rocks. The Na_2O contents remain nearly constant between 1.7 and 2.1 wt % with increasing SiO_2 .

Although the overall rare earth element (REE) abundance of the Gucheng pluton syenites varies significantly (total REE = $5.20\text{--}428.98$ ppm), their light REE (LREE)-enriched chondrite-normalized REE patterns display nearly parallel trends (Fig. 4a), with $(\text{La}/\text{Yb})_{\text{CN}} = 2.81\text{--}22.47$ $(\text{La}/\text{Gd})_{\text{CN}} = 1.41\text{--}6.67$ and $(\text{Gd}/\text{Yb})_{\text{CN}} = 1.98\text{--}3.37$. They show light Eu negative anomalies with δEu values between 0.58 and 0.89 (with one sample having a value of 0.26). In the primitive mantle-normalized multi-element diagrams (Fig. 4b), the analysed Gucheng pluton rocks exhibit coherent, parallel patterns, characterized by enrichment in large ion lithophile elements (LILE; e.g. Rb, Ba, Sr and K) and LREE, and depletion in high field strength elements (HFSE; e.g. Nb, Ta and Ti).

6.b. Mineral chemistry

We present the mineral chemistry of clinopyroxene, feldspar, titanite and garnet from the Gucheng pluton in Supplementary Files 3–6, respectively (online Supplementary Material at <https://doi.org/10.1017/S0016756819000797>).

Clinopyroxene grains in the Gucheng pluton belong to the Ca–Mg–Fe series, and span a compositional range from diopside to hedenbergite and augite ($\text{Wo}_{43\text{--}48}\text{En}_{19\text{--}35}\text{Fs}_{18\text{--}38}$; Fig. 5a), with $\text{SiO}_2 = 49.18\text{--}52.99$ wt %, $\text{Al}_2\text{O}_3 = 0.47\text{--}2.01$ wt %, $\text{CaO} = 18.69\text{--}23.30$ wt %, $\text{Na}_2\text{O} = 0.77\text{--}2.72$ wt %, $\text{TFeO} = 10.09\text{--}20.56$ wt %, and $\text{MgO} = 5.71\text{--}11.90$ wt %.

The Gucheng pluton feldspars form two groups (Fig. 5b): K-feldspar (sanidine; $\text{An}_0\text{Ab}_{3\text{--}11}\text{Or}_{89\text{--}97}$; $\text{SiO}_2 = 64.44\text{--}65.96$ wt %, $\text{K}_2\text{O} = 14.54\text{--}16.23$ wt %, $\text{Na}_2\text{O} = 0.37\text{--}1.13$ wt %) and Na-feldspar (albite; $\text{An}_{0\text{--}3}\text{Ab}_{97\text{--}99}\text{Or}_{0\text{--}1}$; $\text{SiO}_2 = 66.58\text{--}69.79$ wt %, $\text{K}_2\text{O} = 0.07\text{--}0.18$ wt %, $\text{Na}_2\text{O} = 10.07\text{--}11.39$ wt %).

As shown in the backscattered electron images (Fig. 6), K-feldspar grains in K-feldspar-bearing clinopyroxenites are commonly anhedral and interstitial in between relatively euhedral clinopyroxene crystals; parts of some K-feldspar grains are made of Na-feldspar (Fig. 6a). In clinopyroxene-bearing syenites (Fig. 6b, c) and alkali-feldspar syenites (Fig. 6d), K-feldspar grains constitute the cumulate phases, with Na-feldspar grains occurring as an interstitial phase or surrounding K-feldspar grains. These textural and mineralogical observations indicate that Na-feldspars were crystallized at a relatively late stage, when the Na_2O contents of the evolving magmas in a magma chamber were increased.

Euhedral titanite is a common mineral in the K-feldspar-bearing clinopyroxenite and clinopyroxene-bearing syenite of the Gucheng pluton. Its composition is made of $\text{CaO} = 27.44\text{--}29.37$ wt %, $\text{Ti} = 35.56\text{--}38.41$ wt %, $\text{SiO}_2 = 29.88\text{--}31.67$ wt %, $\text{FeO} = 1.43\text{--}2.44$ wt % and $\text{Al}_2\text{O}_3 = 0.34\text{--}1.45$ wt %, and its calculated formula is $\text{Ca}_{0.988\text{--}1.037}\text{Ti}_{0.902\text{--}0.957}[\text{Si}_{1\text{--}1.043}\text{O}_4]\text{O}$.

Garnet locally occurs in K-feldspar-bearing clinopyroxenite and alkali-feldspar syenite rocks. Compositionally, it is made of andradite with $\text{SiO}_2 = 34.08\text{--}35.93$ wt %, $\text{TiO}_2 = 0.43\text{--}1.67$ wt %, $\text{Al}_2\text{O}_3 = 1.93\text{--}3.10$ wt %, $\text{FeO} = 24.62\text{--}26.2$ wt % and $\text{CaO} = 31.08\text{--}31.96$. Its calculated formula is $(\text{Ca}_{2.785\text{--}2.908}\text{Fe}^{2+}_{0.017\text{--}0.139}\text{Mn}_{0.051\text{--}0.111})(\text{Fe}^{3+}_{1.618\text{--}1.838}\text{Al}_{0.165\text{--}0.306})[\text{Si}_{2.898\text{--}3.009}\text{Ti}_{0\text{--}0.102}\text{O}_{12}]$.

6.c. Zircon U–Pb dating and *in situ* zircon oxygen isotopes

We chose an alkali-feldspar syenite sample (GC-1) for U–Pb zircon dating and *in situ* oxygen isotope analysis, because: (i) K-feldspar-bearing clinopyroxenite rocks are composed mainly of clinopyroxene and sanidine, and they have low SiO_2 contents (50.89–56.1 wt %); it is hard to separate a sufficient quantity of zircons from such rocks

Table 1. Major and trace element compositions of Gucheng pluton

Rock	K-fsp clinopyroxenite				Cpx-bearing syenite				Alkali-feldspar syenite		
Sample	GC-57	GC-56-1	GC-56-2	GC-55	GC-50	GC-32	GC-41	GC-52	GC-1	GC-20	GC-39
Major elements (wt %)											
SiO ₂	50.89	53.2	56.1	60.38	60.74	60.96	61.74	62.78	64.06	64.88	65.11
TiO ₂	1.17	1.23	1.1	0.6	0.46	0.47	0.46	0.25	0.06	0.01	0.09
Al ₂ O ₃	3.87	4.32	8.78	14.65	15.25	15.56	15.47	16.68	18.37	18.39	17.03
Fe ₂ O ₃ Total	15.26	12.93	9.56	5.76	4.98	4.81	3.75	2.76	0.97	0.23	1.18
MnO	0.34	0.35	0.23	0.09	0.08	0.07	0.07	0.05	0.02	0	0.02
MgO	7.18	6.62	4.32	1.44	1.31	1.03	1.08	0.68	0.09	0.05	0.28
CaO	16.2	16.18	10.89	3.83	3.23	2.4	3.41	1.89	0.52	0.08	0.83
Na ₂ O	1.71	1.65	1.64	1.85	1.75	1.31	2.02	1.83	1.99	1.98	1.9
K ₂ O	2.03	2.39	6.03	10.25	11.12	12.26	11.02	12.05	12.59	13.38	12.59
P ₂ O ₅	0.5	0.45	0.42	0.23	0.21	0.19	0.17	0.1	0.01	0	0.02
LOI	0.15	0.08	0.09	0.36	0.25	0.26	0.19	0.31	0.51	0.33	0.29
Total	99.3	99.4	99.16	99.44	99.38	99.32	99.38	99.38	99.19	99.33	99.34
δ	1.77	1.60	4.49	8.42	9.34	10.25	9.07	9.74	10.09	10.78	9.50
K ₂ O/Na ₂ O	1.19	1.45	3.68	5.54	6.35	9.36	5.46	6.58	6.33	6.76	6.63
K ₂ O + Na ₂ O	3.74	4.04	7.67	12.1	12.87	13.57	13.04	13.88	14.58	15.36	14.49
Trace element (ppm)											
Sc	60.5	58.1	38.2	14.9	12.2	9.5	9.12	4.91	0.78	<0.05	1.36
V	534	506	346	168	138	122	112	54.5	38.5	4.4	27.8
Cr	68.1	66.4	35	11.8	14.3	153	10.6	9.41	4.71	3.17	6.79
Co	50.3	45.5	31.8	14.1	11.3	11.7	8.95	6.55	0.72	0.17	1.7
Ni	40.5	35.9	21.7	6.88	7.31	68.6	5.28	4.72	1.17	<0.05	1.2
Ga	13.1	13.3	14.2	15.2	16.1	16.5	15.2	14.8	11.9	11.2	15
Rb	28.5	30.9	75.7	142	135	148	118	118	121	149	137
Sr	1757	1591	2459	2902	2650	2363	2772	3277	3861	4807	2355
Y	38.6	42.2	34.8	17.5	14.1	14.2	14	6.34	3.76	0.68	1.95
Zr	74.9	79.8	55.1	23	25.7	26.8	27.1	10.1	11.2	1.83	21.8
Nb	28.9	35.2	31.5	15.3	10.3	12.3	15.3	6.57	1.65	1.13	3.4
Cs	0.07	0.12	0.22	0.46	0.51	0.4	0.4	0.34	0.43	0.47	0.38
Ba	693	777	2081	3222	3241	2250	4000	2639	7184	1899	2997
La	75.2	79.2	72.3	37.2	31.4	29.4	28.3	15	1.54	1.36	2.99
Ce	190	200	174	85.7	68.4	60.9	64	27.9	2.22	2.22	5.8
Pr	20.3	21.1	18.9	9.76	7.7	7.46	7.43	3.78	0.46	0.23	0.9
Nd	76.3	79.2	70.4	36	27.7	27.1	26.5	13.4	2.25	0.89	3.3
Sm	13.4	13.9	12.1	6.22	4.78	4.77	4.59	2.24	0.66	0.18	0.61
Eu	3.6	3.74	3.03	1.34	0.86	0.97	0.98	0.44	<0.05	<0.05	0.05
Gd	10.8	11.4	10	5.28	4.15	3.86	4.06	1.88	0.91	0.18	0.55
Tb	1.58	1.67	1.42	0.73	0.54	0.56	0.57	0.26	0.11	<0.05	0.07
Dy	7.89	8.33	6.97	3.51	2.74	2.91	2.85	1.3	0.65	0.09	0.34
Ho	1.42	1.49	1.23	0.64	0.48	0.52	0.52	0.23	0.12	<0.05	0.06
Er	4.11	4.32	3.61	1.83	1.4	1.48	1.45	0.66	0.41	0.05	0.2
Tm	0.51	0.52	0.43	0.21	0.17	0.18	0.17	0.08	0.05	<0.05	<0.05

(Continued)

Table 1. (Continued)

Rock	K-fsp clinopyroxenite			Cpx-bearing syenite				Alkali-feldspar syenite			
Yb	3.26	3.55	2.8	1.3	1.11	1.12	1.07	0.45	0.37	<0.05	0.17
Lu	0.53	0.56	0.42	0.19	0.15	0.18	0.16	0.06	0.06	<0.05	<0.05
Hf	2.8	2.97	2.16	0.95	0.93	1	1.02	0.38	0.4	0.06	0.57
Ta	1.74	2.04	1.8	0.98	0.67	0.76	0.89	0.38	0.06	<0.05	0.16
Pb	4.02	6.17	10.5	6.83	9.18	3.74	8.69	7.18	13.2	25.5	7.79
Th	5.63	6.14	5.57	3.04	2.51	2.4	2.45	0.88	0.28	0.24	0.73
U	0.68	0.81	0.72	0.32	0.38	0.24	0.53	0.17	0.24	0.06	0.25
(La/Yb) _{CN}	15.55	15.04	17.41	19.29	19.07	17.70	17.83	22.47	2.81		11.86
δEu	0.89	0.88	0.82	0.70	0.58	0.67	0.68	0.64			0.26

δ = (K₂O + Na₂O)²/(SiO₂-43) (units in wt. %); CN stands for chondrite-normalized; normalizing values are from Boynton (1984).

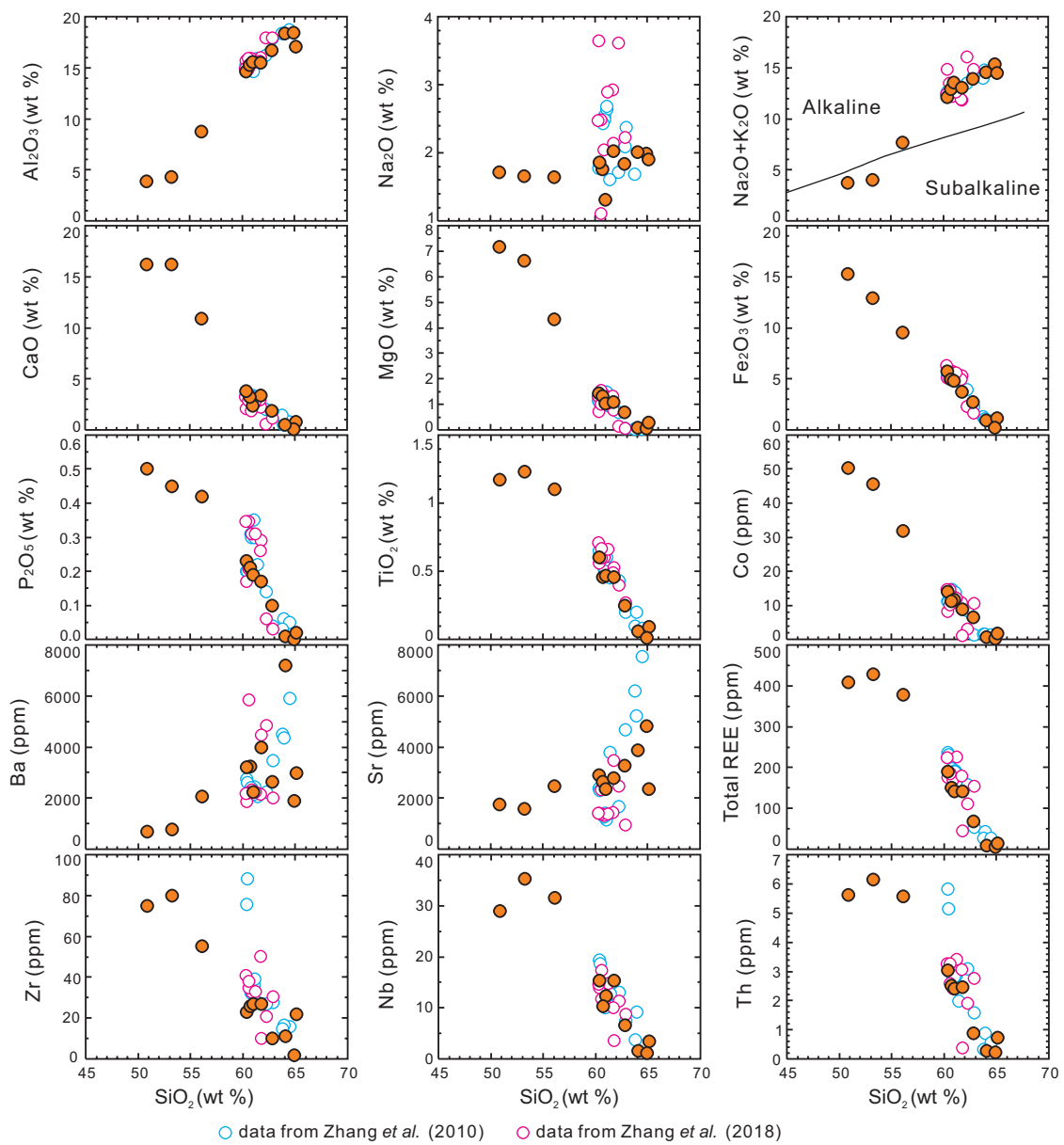


Fig. 3. Plots of major and representative trace element vs SiO₂ contents for the Gucheng pluton.

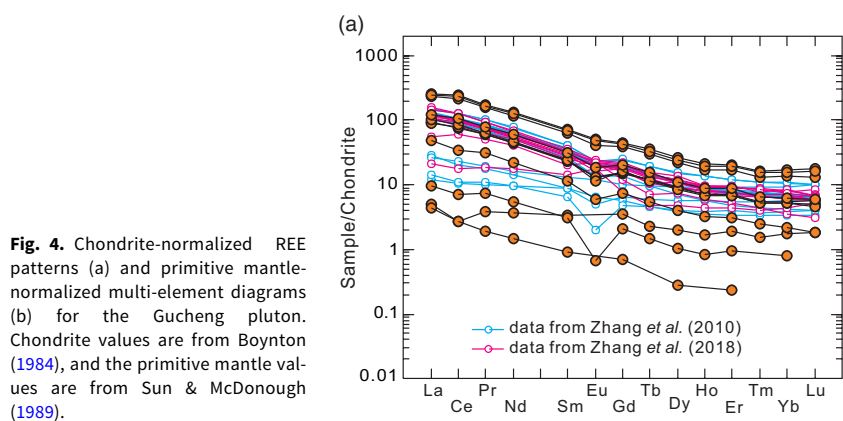


Fig. 4. Chondrite-normalized REE patterns (a) and primitive mantle-normalized multi-element diagrams (b) for the Gucheng pluton. Chondrite values are from Boynton (1984), and the primitive mantle values are from Sun & McDonough (1989).

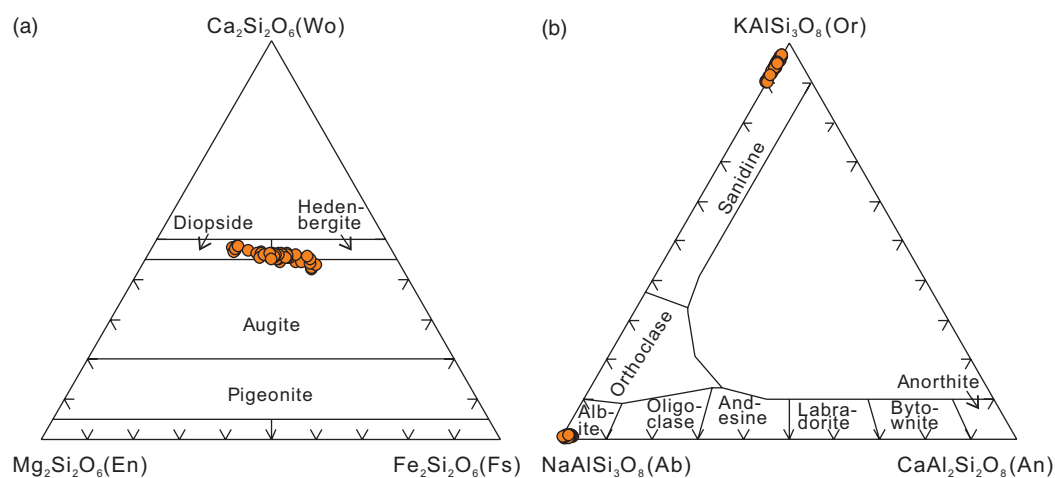


Fig. 5. Classification diagrams of clinopyroxene (a) and feldspar (b) from the Gucheng pluton.

for dating; (ii) XH Zhang *et al.* (2010) and QQ Zhang *et al.* (2018) already dated the zircons from the clinopyroxene-bearing syenite samples, which gave weighted mean $^{206}\text{Pb}/^{238}\text{U}$ ages of 408 ± 4 Ma and 401 ± 2 Ma, respectively. Therefore, we chose the newly discovered, undated alkali-feldspar syenite samples for zircon dating and oxygen isotope analysis. Since the three alkali-feldspar syenite samples have similar elemental compositions and mineralogy, we only chose sample GC-1 for U–Pb zircon dating and *in situ* oxygen isotope analysis.

Zircon grains separated from the alkali-feldspar syenite sample (GC-1) show oscillatory zoning with no inherited cores (Supplementary File 7 in online Supplementary Material at <https://doi.org/10.1017/S0016756819000797>), indicating their magmatic origin. We picked zircons for SHRIMP U–Pb isotope analysis that are transparent and free of visible inclusions. The analytical data are presented in Table 2 and graphically shown in a concordia diagram (Fig. 7). The analysed grains have yielded ^{204}Pb -corrected $^{206}\text{Pb}/^{238}\text{U}$ ages, ranging from 404.0 ± 8.0 Ma to 424.0 ± 8.4 Ma, with a weighted mean $^{206}\text{Pb}/^{238}\text{U}$ age of 415.5 ± 4.5 Ma (14 analyses, MSWD = 0.47). Combined with the zircon U–Pb ages obtained from the clinopyroxene-bearing syenite samples (XH Zhang *et al.* 2010; QQ Zhang *et al.* 2018), we thus interpret the emplacement age of the Gucheng pluton as Early Devonian.

Oxygen isotopic compositions of the analysed zircons are listed in Table 3. The Gucheng pluton zircons have $\delta^{18}\text{O}$ values in the range 5.2 to 6.7 (see Supplementary File 7 in online

Supplementary Material at <https://doi.org/10.1017/S0016756819000797>) for analytical spots in the representative zircon grains).

6.d. Whole-rock Sr and Nd isotopic compositions

Sr and Nd isotopic compositions of the Gucheng plutonic rocks are listed in Table 4. The initial isotopic compositions are calculated at 415 Ma based on the U–Pb zircon age we have obtained in this study. The samples display relatively homogeneous Sr isotopic compositions with initial $^{87}\text{Sr}/^{86}\text{Sr}$ values between 0.7054 and 0.7063, but variable Nd isotopic compositions with $\epsilon_{\text{Nd}}(t)$ ranging from -23.4 to -10.1 (Fig. 8).

7. Petrogenesis, melt evolution and mantle source of the Gucheng pluton

The Gucheng pluton consists of K-feldspar-bearing clinopyroxenite, clinopyroxene-bearing syenite and alkali-feldspar syenite. These rock-types form cyclic intercalations in the outcrop (Fig. 2a), and the boundaries between them are abrupt due to their different mineral assemblages: K-feldspar-bearing clinopyroxenite is composed dominantly of clinopyroxene (>80 %) and minor interstitial K-feldspar, whereas the alkali-feldspar syenite consists predominantly of coarse-grained K-feldspar (>95 %). Three rock-types can be identified in the field and in thin-section based on different proportions of clinopyroxene and K-feldspar in them.

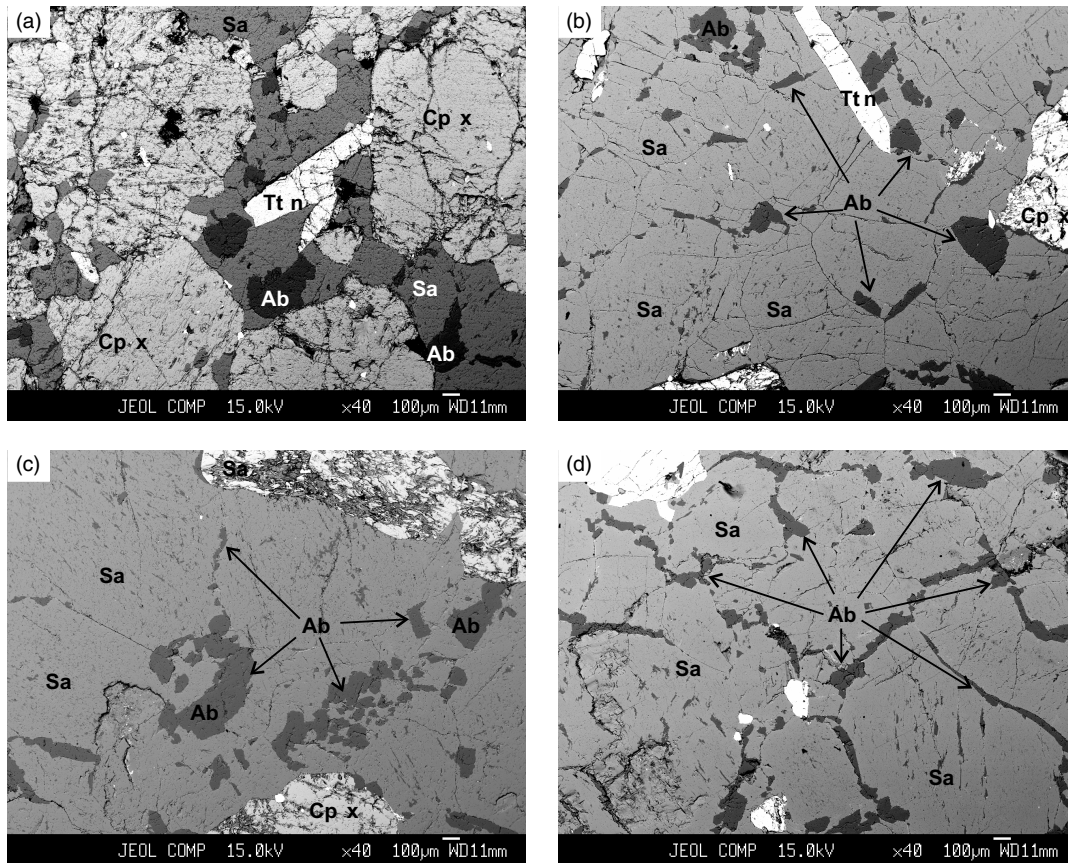


Fig. 6. Backscattered electron (BSE) images of the K-feldspar-bearing clinopyroxenite and clinopyroxene-bearing syenites of the Gucheng pluton. Sa – sanidine; Ab – albite; Cpx – clinopyroxene; Ttn – titanite.

K-feldspar-bearing clinopyroxenite shows typical cumulate textures, characterized by accumulation of coarse-grained, euhedral clinopyroxene with interstitial, anhedral K-feldspar grains. The alkali-feldspar syenite, which is composed of nearly pure K-feldspar, likely formed by the accumulation of K-feldspar, or by the crystallization of residual melt after significant fractionation of clinopyroxene. We interpret the formation of clinopyroxene-bearing syenites as a result of accumulation of clinopyroxene and K-feldspar out of the magma, or as a mixture of cumulus clinopyroxene and residual magma in a magma chamber.

The major and trace elements of the Gucheng pluton rocks vary significantly and regularly (Fig. 3), which is a typical character of cumulate rocks. The LILE (Rb, Ba, Sr, K and Cs) and HFSE (Zr, Hf, Th, U, Nb, Ta and REE) are all incompatible elements, but they behave differently during magma chamber evolution. LILE abundances increase with increasing SiO_2 contents, whereas HFSE abundances decrease significantly (Fig. 3). This phenomenon may be related to different partition coefficients of certain elements between specific minerals (clinopyroxene, K-feldspar, titanite or garnet) and the melt. However, this is a topic of further investigation and is outside the scope of the current study.

7. a. Nature of parental magmas

Although the Gucheng syenitic rocks are of cumulate origin, geochemically they still have relatively high $\text{K}_2\text{O} + \text{Na}_2\text{O}$ contents (3.74–15.36 wt %), high $\text{K}_2\text{O}/\text{Na}_2\text{O}$ ratios (1.19–9.36) and high $(\text{K}_2\text{O} + \text{Na}_2\text{O})^2/(\text{SiO}_2 - 43)$ ratios (1.60–10.78), suggesting their

alkaline, ultrapotassic affinity. The occurrence of normative quartz also indicates that they are SiO_2 -saturated. Their mineral assemblages and mineral chemistry provide important information on the geochemical features of their parental magmas. The Gucheng pluton rocks are composed mainly of diopside–hedenbergite–augite ($\text{Wo}_{43-48}\text{En}_{19-35}\text{Fs}_{18-38}$; Fig. 5a), K-feldspar (sanidine; $\text{An}_0\text{Ab}_{3-11}\text{Or}_{89-97}$; Fig. 5b), subordinate titanite, minor garnet, and Na-feldspar (albite; $\text{An}_{0-3}\text{Ab}_{97-99}\text{Or}_{0-1}$), suggesting a SiO_2 – Al_2O_3 – TiO_2 – CaO – FeO – MgO – K_2O (less Na_2O) chemical system.

These geochemical features and the mineralogy are comparable with those of the Late Triassic ultrapotassic rocks emplaced in the northern margin of the North China Craton. A good example is the Fanshan ultramafic–syenitic complex (Niu *et al.* 2012), which is a typical Late Triassic ultrapotassic intrusion emplaced into the Archaean basement of the North China Craton to the SE of the Gucheng pluton. It consists of ultramafic rocks (clinopyroxenite, glimmerite), garnet–clinopyroxene syenite and alkali-feldspar syenite that formed by fractional crystallization and accumulation of SiO_2 -undersaturated, ultrapotassic alkaline–peralkaline magmas. The Fanshan parental magmas had high contents of CaO, Fe_2O_3 , K_2O , fluid compositions of P_2O_5 , F, CO_2 , H_2O , and had high-temperature, high-oxygen fugacity values. Diopside, melanite (andradite with high TiO_2 contents), biotite, K-feldspar, titanomagnetite, calcite and apatite were the major mineral phases that crystallized out of these magmas (Niu *et al.* 2012).

There are some similarities between the Early Devonian Gucheng pluton and the Late Triassic Fanshan intrusion: (i) clinopyroxenite, clinopyroxene syenite and alkali-feldspar syenite are

Table 2. Zircon SHRIMP U–Th–Pb isotopic data for Gucheng syenite

Spot no.	Abundance (ppm)		Isotopic ratio					Ages (Ma)					
	Th	U	²⁰⁶ Pb*	²⁰⁶ Pb*/ ²³⁸ U	1σ	²⁰⁷ Pb*/ ²³⁵ U	1σ	²⁰⁶ Pb/ ²³⁸ U	1σ	²⁰⁷ Pb/ ²⁰⁶ Pb	1σ	²⁰⁸ Pb/ ²³² Th	1σ
GC-1-1	1045	54	60.7	0.0675	0.0014	0.518	0.012	421.1	8.3	439	22	413	25
GC-1-2	545	54	31.5	0.0671	0.0014	0.505	0.014	418.6	8.4	397	41	371	29
GC-1-3	937	55	52.2	0.0647	0.0013	0.474	0.012	404	8	337	35	298	40
GC-1-4	456	29	26.1	0.0664	0.0014	0.505	0.015	414.6	8.3	419	49	346	54
GC-1-5	359	30	20.9	0.0675	0.0015	0.518	0.015	420.8	9	442	41	426	29
GC-1-6	626	58	35.3	0.0657	0.0014	0.487	0.012	410	8.2	361	27	352	14
GC-1-7	692	97	39.9	0.067	0.0014	0.506	0.012	418.1	8.3	404	28	408	14
GC-1-8	592	34	33.9	0.0666	0.0014	0.505	0.012	415.6	8.3	413	29	395	27
GC-1-9	762	15	43.7	0.0666	0.0013	0.507	0.012	415.8	8.2	419	24	527	44
GC-1-10	897	113	50.8	0.0659	0.0013	0.508	0.011	411.3	8.1	451	21	403	11
GC-1-11	816	34	47.7	0.068	0.0014	0.512	0.012	424	8.4	396	29	436	35
GC-1-12	714	36	41.6	0.0678	0.0014	0.521	0.013	422.9	8.4	441	28	424	32
GC-1-13	522	42	29.6	0.0658	0.0014	0.495	0.014	411	8.2	394	42	354	35
GC-1-14	426	29	24.2	0.0659	0.0014	0.499	0.014	411.2	8.9	409	41	372	37

Errors are 1-sigma; Pb* indicate the radiogenic portions. Common Pb corrected using measured ²⁰⁴Pb.

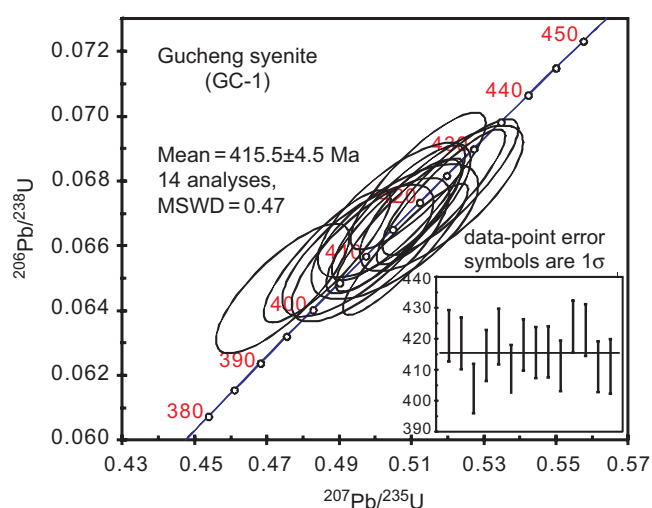


Fig. 7. Concordia diagram showing the zircon age data. Inset shows the weighted mean ²⁰⁶Pb/²³⁸U age.

the dominant rock-types in both; (ii) diopside and K-feldspar are the dominant mineral phases in both; and (iii) fractional crystallization and crystal accumulation were the main processes in the evolution of their magmas. However, there are still some major differences between these two ultrapotassic plutons: biotite, melanite, calcite and titanomagnetite are abundant in the Fanshan intrusion, whereas they are absent in the Gucheng pluton. Parental magmas of the Gucheng pluton were ultrapotassic, alkaline and had high contents of CaO, FeO, K₂O and TiO₂ and low contents of Na₂O. However, when compared with the Late Triassic Fanshan intrusion, the parental magmas of the Gucheng pluton were SiO₂-saturated, less alkaline and had low contents of fluid compositions (H₂O, CO₂), low oxygen fugacities and low temperatures, resulting in the absence of minerals such as biotite, melanite and calcite in the Gucheng plutonic rocks.

7.b. Metasomatized, enriched mantle source of the Gucheng pluton magmas

The K-feldspar-bearing clinopyroxenite, clinopyroxene-bearing syenite and alkali-feldspar syenite of the Gucheng pluton show continental crust-like trace element patterns and Sr–Nd isotopic signatures. The Gucheng pluton rocks have high Th/Yb ratios above the MORB–ocean island basalt (MORB–OIB array; Fig. 9), and have radiogenic Sr isotopic compositions (initial ⁸⁷Sr/⁸⁶Sr = 0.7054–0.7063) and negative $\epsilon_{\text{Nd}}(t)$ values (–23.4 to –10.1). Such trace element and Sr–Nd characteristics may result from partial melting of a lithospheric mantle, which was previously enriched by subduction-related metasomatism, or from contamination of depleted mantle-derived magmas by crustal components during their ascent to the crustal levels.

However, our calculations based on a simple two-component mixing model (Langmuir *et al.* 1978) demonstrate that mixing between parental magmas, derived from a depleted mantle source (Sr = 150 ppm, ⁸⁷Sr/⁸⁶Sr = 0.704, Nd = 6 ppm, $\epsilon_{\text{Nd}} = 10$; Rudnick *et al.* 2004), with an Archaean crustal component (representative tonalite–trondhjemite–granodiorite gneisses in the North China Craton have most radiogenic Sr isotopic ratios and lowest ϵ_{Nd} values; Sr = 320 ppm, ⁸⁷Sr/⁸⁶Sr = 0.716, Nd = 27 ppm, $\epsilon_{\text{Nd}} = -35$; Jahn *et al.* 1987; Zhang *et al.* 1991), cannot explain the observed Sr–Nd isotope compositions of the analysed samples (Fig. 8). Therefore, the Gucheng pluton syenites were unlikely to have originated from a depleted MORB-type mantle source. Instead, the Gucheng pluton magmas were derived from partial melting of an enriched subcontinental lithospheric mantle. This inference is consistent with the occurrence of an isotopically enriched subcontinental lithospheric mantle beneath the North China Craton in the Palaeozoic, as revealed by the studies of upper mantle xenoliths recovered from the Ordovician kimberlites (Zheng & Lu, 1999).

The Sr isotopic compositions of the Gucheng pluton rocks should resemble those of their mantle source. Although magma-fractionation process could result in the increase of Sr contents

Table 3. Zircon *in situ* oxygen isotope compositions for the Gucheng syenite

Spot no.	$\delta^{18}\text{O}_{\text{V-SMOW}}$ (‰)	1 σ
GC-1-1	5.57	0.17
GC-1-2	5.20	0.25
GC-1-3	5.22	0.14
GC-1-4	5.97	0.29
GC-1-5	5.97	0.35
GC-1-6	5.75	0.31
GC-1-7	6.66	0.18
GC-1-8	5.67	0.25
GC-1-9	6.23	0.33
GC-1-10	6.45	0.16
GC-1-11	5.84	0.18
GC-1-12	5.25	0.26
GC-1-13	6.05	0.18
GC-1-14	5.81	0.23
GC-1-15	5.72	0.34
GC-1-16	5.66	0.26
GC-1-17	5.87	0.12
GC-1-18	5.75	0.15
GC-1-19	5.82	0.12
GC-1-20	6.07	0.13
GC-1-21	5.88	0.22

$\delta^{18}\text{O}_{\text{V-SMOW}} = [({}^{18}\text{O}/{}^{16}\text{O})_{\text{sample}}/({}^{18}\text{O}/{}^{16}\text{O})_{\text{V-SMOW}} - 1] \times 1000$; $({}^{18}\text{O}/{}^{16}\text{O})_{\text{V-SMOW}} = 0.0020052$, Vienna Standard Mean Ocean Water (V-SMOW) standard.

(Fig. 3), for the Gucheng rocks, the sample (GC-57, K-feldspar-bearing clinopyroxenite) with the lowest SiO_2 content (50.89 wt %) still has higher Sr content (1757 ppm) than those of crustal rocks (average 320 ppm; Rudnick & Gao, 2003). Having high Sr contents is a typical character of ultrapotassic rocks (e.g. Niu *et al.* 2012, 2017; Conticelli *et al.* 2015), which should be related to their mantle source mineralogy and partial melting degrees. The high Sr contents of the Gucheng pluton make their Sr isotopic compositions immune to possible crustal contamination effects. This inference is consistent with the relatively homogeneous Sr isotopic ratios of the Gucheng pluton rocks.

The radiogenic Sr isotopic compositions of the Gucheng pluton rocks can be attributed to recycling of subducted sediments into their mantle source, causing subduction metasomatism and enrichment (Plank & Langmuir, 1998). A simple calculation based on a two-component mixing model (Langmuir *et al.* 1978) indicates that incorporation of c. 9–25 % sediments (represented by global subducting sediment with $\text{Sr} = 380$ ppm, ${}^{87}\text{Sr}/{}^{86}\text{Sr} = 0.718$; Plank & Langmuir, 1998) to the subcontinental lithospheric mantle beneath the North China Craton (represented by kimberlite-hosted xenoliths with $\text{Sr} = 600$ ppm, ${}^{87}\text{Sr}/{}^{86}\text{Sr} = 0.7045$; Zheng & Lu, 1999) can successfully achieve the Sr isotopic compositions of the Gucheng pluton magmas, and thus their mantle melt source (Fig. 8).

Studies of the petrogenesis of many other ultrapotassic plutonic and volcanic rocks worldwide have shown that sediment recycling into the mantle source may have indeed played an important role

in the formation of their magmas (e.g. Conticelli & Peccerillo, 1992; Nelson, 1992; Conticelli *et al.* 2007, 2015; Avanzinelli *et al.* 2009; Dilek & Altunkaynak 2010; Tommasini *et al.* 2011; Prelević *et al.* 2012; Mallik *et al.* 2015). Fluids or melts derived from subducted sediments on downgoing oceanic plates percolate through the peridotites in the mantle wedge and react with olivine during their ascent, producing K-amphibole, phlogopite, orthopyroxene and clinopyroxene containing, enriched silicate melt (e.g. Sekine & Wyllie, 1983; Bianchini *et al.* 2011). Precipitation of this melt in extensive vein networks within the mantle wedge then creates highly metasomatized peridotites (Foley 1992). Partial melting of such metasomatized veins could produce ultrapotassic magmas (e.g. Brey & Green 1977; Brey *et al.* 2008; Foley *et al.* 2009; Conticelli *et al.* 2015). The Gucheng pluton rock samples have low Th/Nb ratios, which might be indicative of recycled sediments within their mantle source mainly as aqueous fluids rather than melts. This inference is supported by the presence of Th-hosted minerals (allanite and/or monazite) in the residue of recycled sediments, which underwent partial melting at the interface between the subducting slab and the overlying mantle wedge (e.g. Klimm *et al.* 2008; Skora & Blundy 2010; Martindale *et al.* 2013).

Rocks of the Gucheng pluton show, however, significantly negative, varied Nd isotopic compositions with their $\epsilon_{\text{Nd}}(t)$ values ranging from -23.4 to -10.1 ; these numbers are much lower than the calculated $\epsilon_{\text{Nd}}(t)$ values based on a model of mixing of subcontinental lithospheric mantle derived melts with melts from global subducting sediments (Fig. 8). This phenomenon may be attributed to crustal contamination of parental magmas during their ascent through and emplacement in the continental crust.

Crustal contamination of the Gucheng pluton magmas is evidenced by the *in situ* oxygen isotopic compositions of zircons. Sample GC-1 zircons display $\delta^{18}\text{O}$ values of 5.2 to 6.7 (Table 3), which are higher than the $\delta^{18}\text{O}$ values of mantle zircons (5.3 ± 0.3); however, these values are close to the oxygen isotope values of zircons in continental crustal rocks ($\delta^{18}\text{O} = 6.5\text{--}7.5$; Valley *et al.* 2005). This observation indicates crustal contamination of the parental magmas of the Gucheng pluton during their transport through the lower and upper crust of the North China Craton.

Possible crustal contaminants for the Gucheng pluton magmas were the Precambrian mafic granulites and amphibolites or tonalite-trondhjemite-granodiorite gneisses that collectively constitute the crystalline basement of the North China Craton (Jahn *et al.* 1987). The mafic lower crust of the North China Craton has Nd isotopic compositions ($\epsilon_{\text{Nd}} = -12$ to -24 ; Zhang *et al.* 1998; Zhou *et al.* 2002; Liu *et al.* 2004) roughly similar to those of the Gucheng pluton, indicating that the mafic lower crustal rocks were unlikely to be the main contaminant, because this would require an addition of unreasonably high proportions of mafic granulites and amphibolites that would have significantly modified the compositions of the Gucheng pluton parental magmas. On the contrary, the tonalite-trondhjemite-granodiorite gneisses have dramatically lower ϵ_{Nd} values ($\epsilon_{\text{Nd}} = -25$ to -40 ; Jahn *et al.* 1987; Zhang *et al.* 1991) than those of the Gucheng pluton, suggesting that the tonalite-trondhjemite-granodiorite gneisses could be the potential contaminants for the Gucheng pluton parental magmas.

8. Tectonomagmatic evolution of the Gucheng pluton: a new model

The existing models for the formation of the Early Devonian alkaline plutons in the northern North China Craton suggest as

Table 4. Rb–Sr and Sm–Nd isotopic data of Gucheng pluton

Sample	Rb	Sr	⁸⁷ Rb/ ⁸⁶ Sr	⁸⁷ Sr/ ⁸⁶ Sr	2σ	(⁸⁷ Sr/ ⁸⁶ Sr) _i	Sm	Nd	¹⁴⁷ Sm/ ¹⁴⁴ Nd	¹⁴³ Nd/ ¹⁴⁴ Nd	2σ	ε _{Nd} (0)	ε _{Nd} (t)	f _{Sm/Nd}
	(ppm)	(ppm)				(415 Ma)	(ppm)	(ppm)						
GC-57	28.5	1757	0.0458	0.706204	4	0.7059	13.4	76.3	0.1114	0.511434	2	−23.5	−19.0	−0.43
GC-56-1	30.9	1591	0.0549	0.706258	14	0.7059	13.9	79.2	0.1113	0.511455	2	−23.1	−18.6	−0.43
GC-56-2	75.7	2459	0.0870	0.706316	4	0.7058	12.1	70.4	0.1090	0.511474	2	−22.7	−18.1	−0.45
GC-55	142	2902	0.1382	0.706681	5	0.7059	6.22	36.0	0.1096	0.511532	2	−21.6	−17.0	−0.44
GC-50	135	2650	0.1439	0.706860	14	0.7060	4.78	27.7	0.1095	0.511885	2	−14.7	−10.1	−0.44
GC-32	148	2363	0.1769	0.706748	4	0.7057	4.77	27.1	0.1117	0.511536	3	−21.5	−17.0	−0.43
GC-41	118	2772	0.1202	0.706977	3	0.7063	4.59	26.5	0.1099	0.511467	4	−22.8	−18.3	−0.44
GC-52	118	3277	0.1017	0.706332	4	0.7057	2.24	13.4	0.1061	0.511514	6	−21.9	−17.1	−0.46
GC-39	137	2355	0.1643	0.707113	5	0.7061	0.61	3.30	0.1173	0.511224	5	−27.6	−23.4	−0.40
GC-20	149	4807	0.0876	0.705890	3	0.7054	0.18	0.89	0.1283					
GC-1	121	3861	0.0885	0.706281	4	0.7058	0.66	2.25	0.1861					

ε_{Nd} = [(¹⁴³Nd/¹⁴⁴Nd)_s/(¹⁴³Nd/¹⁴⁴Nd)_{CHUR} − 1] × 10 000, f_{Sm/Nd} = (¹⁴⁷Sm/¹⁴⁴Nd)_s/(¹⁴⁷Sm/¹⁴⁴Nd)_{CHUR} − 1, where (¹⁴³Nd/¹⁴⁴Nd)_s and (¹⁴⁷Sm/¹⁴⁴Nd)_s are the measured values of samples (¹⁴³Nd/¹⁴⁴Nd)_{CHUR} = 0.512638 and (¹⁴⁷Sm/¹⁴⁴Nd)_{CHUR} = 0.1967.

a driving mechanism post-collisional magmatism (Huang & Hou, 2017) or slab break-off associated with the subduction of the Palaeo-Asian Ocean lithosphere beneath the North China Craton (Zhang *et al.* 2010). However, neither of these models is compatible with the regional geology. The post-collisional magmatism idea envisions the onset of alkaline magmatism nearly 60 million years after the collisional accretion of the Ulan island arc into the North China Craton continental margin, but this is an unreasonably long period of time for collision-driven lithospheric foundering (Pysklywec *et al.* 2002; Dilek & Altunkaynak 2007; Shaffer *et al.* 2017). The slab break-off model envisages the detachment of the downgoing Palaeo-Asian Ocean slab and suggests that slab break-off-induced asthenospheric upwelling might have caused the necessary partial melting of the subcontinental lithospheric mantle (Zhang *et al.* 2010). However, these authors provide no explanation for the cause of the inferred slab break-off, and the regional geology does not provide any evidence or a reason (i.e. attempted subduction of a microcontinent or an oceanic plateau in the downgoing Palaeo-Asian slab) that could have led to the detachment and sinking of the negatively buoyant oceanic slab. Many well-developed slab break-off induced magmatic events in different orogenic belts show unequivocal geological and geophysical evidence for attempted and partial subduction of positively buoyant continental blocks/plates or large seamounts in downgoing oceanic plates (Davies & Blanckenburg, 1995; Hildebrand & Bowring, 1999; Dilek & Whitney 2000; Dilek 2003; Cloos *et al.* 2005; Dilek & Altunkaynak, 2007; Dilek & Sandvol, 2009; Dilek *et al.* 2010).

We present a new tectonomagmatic model for the Early Devonian alkaline magmatism in the northern part of the North China Craton that is compatible with the extant geological data and the geochemical and geochronological constraints as documented in our study here. Following the Early Ordovician collision of the Ulan intraoceanic arc system with the passive margin of the North China Craton (Fig. 10A, B), subduction jump and polarity flip resulted in the beginning of an Andean-type active continental margin tectonics as the Palaeo-Asian Ocean lithosphere started subducting southwards beneath the North China Craton (Fig. 10B). We posit that initially this subduction zone had a shallow dip angle because of the very large width of the downgoing Palaeo-Asian

Ocean slab (Schellart *et al.* 2010; Dilek & Tang, 2019). This inferred shallow subduction resulted in the development of the early Bainaimiao continental arc (~470 Ma) farther inboard from the trench. Pelitic and volcanoclastic sediments, which were deposited earlier in a back-arc environment of the Ulan island arc system, became subducted and underwent partial melting at the interface of the shallow slab, producing K- and silica-rich metasomatic fluids with residual garnet, rutile, allanite and/or monazite. These metasomatic fluids infiltrated into and reacted with the overlying subcontinental lithospheric mantle beneath the North China Craton, forming phlogopite-, K-amphibole- and orthopyroxene-rich vein networks (Fig. 10B1).

Subsequent slab rollback and steepening of the subduction zone induced asthenospheric flow and heat flux, causing partial melting of these metasomatic veins in the subcontinental lithospheric mantle that produced the ultra-alkaline magmas of the Gucheng pluton around 415–405 Ma (Fig. 1c). With increased asthenospheric heat flux and slab-derived fluids the host peridotites of metasomatic veins also experienced partial melting, contributing subduction-influenced melts into the melt regime of the Gucheng pluton. Flux melting of the mantle wedge peridotites above the more steeply dipping Palaeo-Ocean slab contributed to calc-alkaline melt/magma evolution of the northward-migrating magmatism in and across the Bainaimiao magmatic arc (Fig. 1c). The Nb/La vs La/Yb diagram in Figure 10C1 shows that both asthenospheric mantle and mixed asthenospheric–lithospheric mantle melt input was important in the evolution of the Gucheng pluton magmas. High (La/Sm)_{PM} and (Tb/Yb)_{PM} ratios of the Gucheng pluton rocks also indicate low-degree partial melting of a garnet-bearing mantle source at great depths in the subcontinental lithospheric mantle (Fig. 10C2).

Extensive fractional crystallization and clinopyroxene accumulation in a magma chamber in the upper crust led to the formation of K-feldspar-bearing clinopyroxenite, whereas accumulation of K-feldspar, or crystallization of the residual melt, led to the formation of alkali-feldspar syenite (Fig. 10C3). The clinopyroxene-bearing syenites in the Gucheng pluton may have resulted from accumulation of clinopyroxene and K-feldspar, or mixing of cumulus clinopyroxene with the residual melt. Spatial relationships among these three rock types in the field suggest that

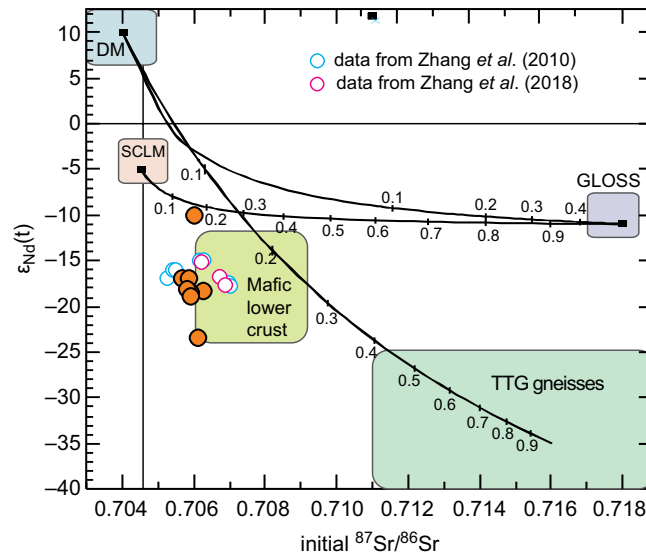


Fig. 8. Plot of $\epsilon_{Nd}(t)$ vs initial $^{87}Sr/^{86}Sr$ ratios for the Gucheng pluton. Nd–Sr isotopic modelling based on a two-component mixing model (Langmuir *et al.* 1978). Also displayed on this plot are the Sr–Nd isotopic compositions of a depleted mantle source (DM; Rudnick *et al.* 2004), Palaeozoic lithospheric mantle beneath the North China Craton (SCLM; Zheng & Lu, 1999), mafic lower crust of the North China Craton (Zhang *et al.* 1998; Zhou *et al.* 2002; Liu *et al.* 2004), tonalite–trondhjemite–granodiorite gneisses (TTG gneisses; Jahn *et al.* 1987; Zhang *et al.* 1991), and global subducting sediment (GLOSS; Plank & Langmuir, 1998) for comparison. Ticks on the lines represent 10 % interval.

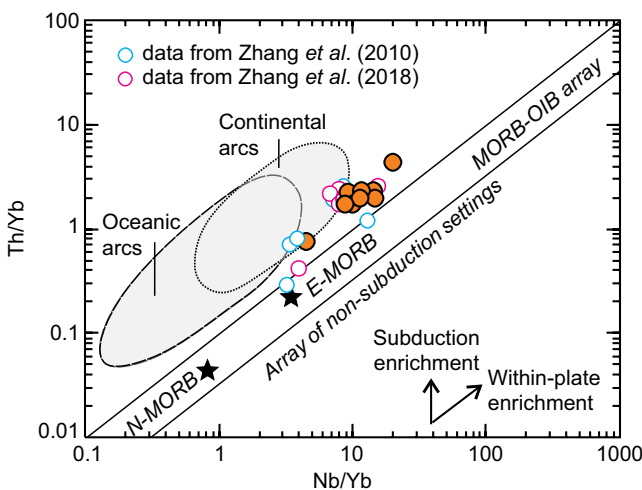


Fig. 9. Plot of Th/Yb vs Nb/Yb for the Gucheng pluton. The compositions of different end members are after McDonough (1990) and Pearce & Peate (1995).

intrusion of alkali-feldspar syenite took place later than the crystallization of the K-feldspar-bearing clinopyroxenite and clinopyroxene-bearing syenite (Fig. 2a).

Emplacement of the alkaline Gucheng pluton in the Early Devonian represented the early stages of incipient continental back-arc magmatism and accompanying extension in the northern part of the North China Craton. This early-stage continental back-arc magmatism was fully developed by the Late Devonian, producing a nearly continuous, E–W-trending belt of alkaline to calc-alkaline plutons to the south of the Bainaimiao magmatic arc.

9. Conclusions

The syenitic Gucheng pluton in the northern part of the North China Craton represents the earliest phase of alkaline magmatism,

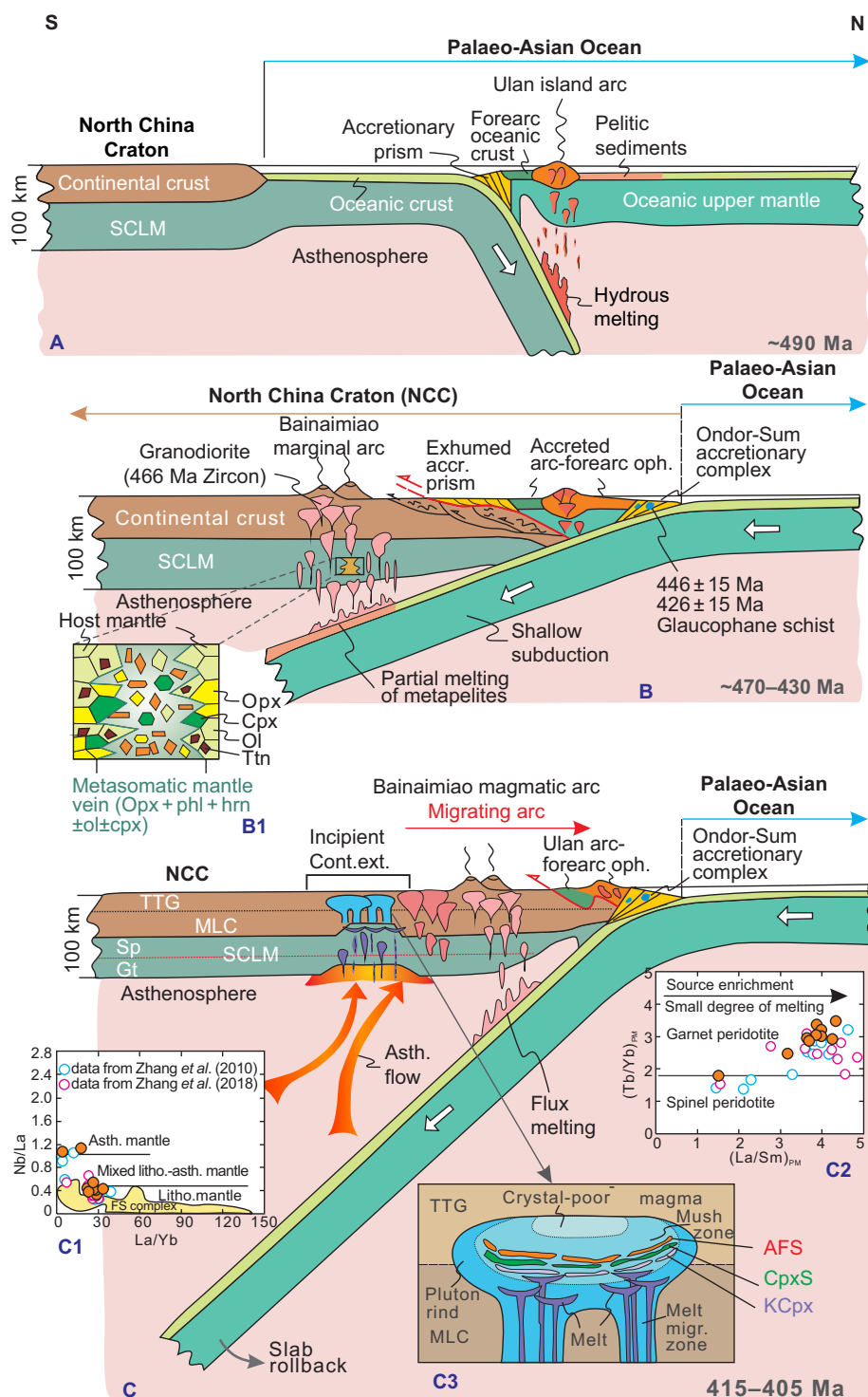
which evolved through punctuated episodes in the Middle Palaeozoic, Late Triassic and latest Jurassic – Early Cretaceous. Our SHRIMP U–Pb dating of its syenitic rock has revealed a crystallization age of 415 Ma for the emplacement of this pluton into the Archaean basement of the North China Craton. It consists mainly of K-feldspar-bearing clinopyroxenite, clinopyroxene-bearing syenite and alkali-feldspar syenite that formed through fractional crystallization and accumulation of ultrapotassic, alkaline parental magmas.

The geochemical and isotopic characteristics of the Gucheng pluton rocks indicate enrichment of their magmas in high Th/Yb ratios, high Sr abundances (higher than average crustal rocks), variable Nd compositions, and *in situ* oxygen $\delta^{18}O$ values that are higher than those of mantle zircons. Collectively, these features suggest that the ultrapotassic Gucheng pluton magmas were derived from partial melting of metasomatic vein networks in the subcontinental lithospheric mantle of the North China Craton. Subducted pelitic sediments on the Palaeo-Asian Ocean slab were the main source of hydrous silicate melts, which made up these alkaline veins in the overlying subcontinental lithospheric mantle. Asthenospheric upwelling driven by slab rollback and steepening provided the necessary heat flux to cause partial melting of metasomatic veins and the production of ultrapotassic magmas of the Gucheng pluton. This mechanism rules out slab break-off related asthenospheric upwelling as the cause of partial melting, as proposed in earlier models.

Acknowledgements. We wish to thank Xiaochao Che and Chunyan Dong for their assistance in zircon U–Pb dating and zircon *in situ* oxygen isotope analyses, and Xiaohong Mao and Mingchun Yang for their assistance in mineral chemistry and Nd–Sr isotope analyses. This research has been financially supported by grants from the Nature Science Foundation of China (Grant Nos. 41672063, 41773029, 41302038 and 41720104009). We acknowledge the critical and helpful reviews by two anonymous referees that helped us improve our interpretations.

Supplementary material. To view supplementary material for this article, please visit <https://doi.org/10.1017/S0016756819000797>.

Fig. 10. Interpretive chemical geodynamics model, depicting a time-progressive development of the Middle Palaeozoic evolution of the northern continental margin of the North China Craton and its magmatism. Notice the geodynamic switch from a collisional to accretionary continental margin tectonics between 490 Ma and 470 Ma. **A** – Intraoceanic development of the Ulan island arc complex in the Palaeo-Asian Ocean, with fore-arc oceanic lithosphere formation and deposition of pelitic and volcanoclastic sediments in a back-arc tectonic setting. **B** – Inception of the shallow subduction of a Palaeo-Asian Ocean slab, following the collisional accretion of the Ulan island arc complex into the continental margin of the North China Craton. U–Pb zircon ages of 466 Ma from a granodiorite pluton in the Bainaimiao continental arc mark the earliest stages of subduction zone magmatism far inland from the trench and nearly time-equivalent Ondor–Sum accretionary complex farther north. **B1** – Emplacement of metasomatic veins derived from partial melting of subducted metapelites at the shallow slab interface into the subcontinental lithospheric mantle peridotites of the North China Craton. **C** – Slab rollback and the associated slab steepening cause the continental arc magmatism represented by the Bainaimiao arc to migrate northwards in the upper plate. Slab-rollback-induced asthenospheric flow results in heat and melt flux into the subcontinental lithospheric mantle that in turn leads into partial melting of metasomatic veins in the subcontinental lithospheric mantle peridotites and hence production of ultra-alkaline magmas, forming the Gucheng pluton. **C1** – Nb/La vs La/Yb diagram displaying the mantle source (asthenospheric vs lithospheric) of the Gucheng pluton magmas. **C2** – (Tb/Yb)_{PM} vs (La/Sm)_{PM} diagram, showing the garnet vs spinel stability field of the source mantle, and the relative degrees of source enrichment and degree of melting. PM = Primitive mantle. **C3** – Inferred magma chamber model for the development of the Gucheng pluton magmas through melt migration, replenishment and fractional crystallization processes. AFS = alkali-feldspar syenite; CpxS = clinopyroxene-bearing syenite; KCpx = K-feldspar-bearing clinopyroxenite; MLC = mafic lower crust; TTG = tonalite–trondhjemite–granodiorite. In the plot of Nb/La vs La/Yb, the black lines separating fields of lithospheric, asthenospheric and mixed lithospheric–asthenospheric mantle are from Abdel-Rahman (2002); the area of Fanshan (FS) complex is from Niu *et al.* (2012). In the plot of (Tb/Yb)_{PM} vs (La/Sm)_{PM}, the boundary between melting products of garnet- and spinel-bearing peridotites is from Wang *et al.* (2002).



References

- Abdel-Rahman AM (2002) Mesozoic volcanism in the Middle East: geochemical, isotopic and petrogenetic evolution of extension-related alkali basalts from central Lebanon. *Geological Magazine* **139**, 621–40.
- Altunkaynak Ş, Sunal G, Aldanmaz E, Genç CS, Dilek Y, Furnes H, Foland KA, Yang J-S and Yildiz M (2012) Eocene granitic magmatism in NW Anatolia (Turkey) revisited: new implications from comparative zircon SHRIMP U–Pb and $^{40}\text{Ar}/^{39}\text{Ar}$ geochronology and isotope geochemistry on magmagenesis and emplacement. *Lithos* **155**, 289–309. doi: 10.1016/j.lithos.2012.09.008.

- Avanzinelli R, Lustrino M, Mattei M, Melluso L and Conticelli S (2009) Potassic and ultrapotassic magmatism in the circum-Tyrrhenian region: significance of carbonated pelitic vs. pelitic sediment recycling at destructive plate margins. *Lithos* **113**, 213–17.
- Bianchini G, Beccaluva L, Nowell GM, Pearson DG and Siena F (2011) Mantle xenoliths from Tallante (Betic Cordillera): insights into the multi-stage evolution of the south Iberian lithosphere. *Lithos* **124**, 308–18.
- Boynton WV (1984) Geochemistry of the earth elements: meteorite studies. In *Rare Earth Element Geochemistry* (ed. P Henderson). New York: Elsevier, pp. 63–114.

- Brey G and Green DH** (1977) Systematic study of liquidus phase relations in olivine melilitite + H₂O + CO₂ at high pressures and petrogenesis of an olivine melilitite magma. *Contributions to Mineralogy and Petrology* **61**, 141–62.
- Brey GP, Bulatov VK, Girnits AV and Lahaye Y** (2008) Experimental melting of carbonated peridotite at 6–10 GPa. *Journal of Petrology* **49**, 797–821.
- Chen B, Jahn BM and Tian W** (2009) Evolution of the Solonker suture zone: constraints from zircon U–Pb ages, Hf isotopic ratios and whole-rock Nd–Sr isotope compositions of subduction- and collision-related magmas and forearc sediments. *Journal of Asian Earth Sciences* **34**, 245–57.
- Chen B, Niu XL, Wang ZQ, Gao L and Wang C** (2013) Geochronology, petrology, and geochemistry of the Yaojiazhuang ultramafic-syenitic complex from the North China Craton. *Science China – Earth Science* **56**, 1294–1307.
- Cloos M, Sapiie B, Van Ufford, AQ, Weiland RJ, Warren PQ and McMahon TP** (2005) *Collisional Delamination in New Guinea: The Geotectonics of Subducting Slab Breakoff*. Boulder, Colorado: Geological Society of America Special Paper 400, 48 pp.
- Coticelli S, Avanzinelli R, Ammannati E and Casalini M** (2015) The role of carbon from recycled sediments in the origin of ultrapotassic igneous rocks in the Central Mediterranean. *Lithos* **232**, 174–90.
- Coticelli S, Carlson RW, Widom E and Serri G** (2007) Chemical and isotopic composition (Os, Pb, Nd, and Sr) of Neogene to Quaternary calc-alkalic, shoshonitic, and ultrapotassic mafic rocks from the Italian peninsula: inferences on the nature of their mantle sources. In *Cenozoic Volcanism in the Mediterranean Area* (eds L Beccaluva, G Bianchini and M Wilson), pp. 171–202. Boulder, Colorado: Geological Society of America Special Paper 418.
- Coticelli S and Peccerillo A** (1992) Petrology and geochemistry of potassic and ultrapotassic volcanism in central Italy: petrogenesis and inferences on the evolution of the mantle sources. *Lithos* **28**, 221–40.
- Davies JH and Blanckenburg F von** (1995) Slab breakoff: a model of lithospheric detachment and its test in the magmatism and deformation of collisional orogens. *Earth and Planetary Science Letters* **29**, 85–102.
- Dilek Y** (2003) Ophiolites, plumes and orogeny. In *Ophiolites in Earth History* (eds Y Dilek and PT Robinson), pp. 9–19. Geological Society of London, Special Publication no. 218.
- Dilek Y and Altunkaynak Ş** (2007) Cenozoic crustal evolution and mantle dynamics of post-collisional magmatism in western Anatolia. *International Geology Review* **49**, 431–53.
- Dilek Y and Altunkaynak Ş** (2010) Geochemistry of Neogene–Quaternary alkaline volcanism in western Anatolia, Turkey and implications for the Aegean mantle. *International Geology Review* **52**, 631–55. doi: [10.1080/00206810903495020](https://doi.org/10.1080/00206810903495020).
- Dilek Y and Furnes H** (2011) Ophiolite genesis and global tectonics: geochemical and tectonic fingerprinting of ancient oceanic lithosphere. *Geological Society of America Bulletin* **123**, 387–411.
- Dilek Y and Furnes H** (2014) Ophiolites and their origins. *Elements*, **10**, 93–100. doi: [10.2113/gselements.10.2.93](https://doi.org/10.2113/gselements.10.2.93).
- Dilek Y, Imamverdiyev N and Altunkaynak Ş** (2010) Geochemistry and tectonics of Cenozoic volcanism in the Lesser Caucasus (Azerbaijan) and the peri-Arabian region: collision-induced mantle dynamics and its magmatic fingerprint. *International Geology Review* **52**, 536–78.
- Dilek Y and Sandvol E** (2009) Seismic structure, crustal architecture and tectonic evolution of the Anatolian–African plate boundary and the Cenozoic orogenic belts in the Eastern Mediterranean Region. In *Ancient Origins and Modern Analogues* (eds JB Murphy, JD Keppie and A Hynes), pp. 127–60. Geological Society of London, Special Publication no. 327. doi: [10.1144/SP327.8](https://doi.org/10.1144/SP327.8).
- Dilek Y and Tang L** (2019) Cordilleran-style tectonomagmatic evolution of Mesozoic SE China through a tectonic mode switch. *Geological Magazine*, this issue.
- Dilek Y and Whitney DL** (2000) Cenozoic crustal evolution in central Anatolia: extension, magmatism and landscape development. In *Proceedings of the Third International Conference on the Geology of the Eastern Mediterranean* (eds I Panayides, C Xenophontos and J Malpas), pp. 183–92. Nicosia: Geological Survey Department.
- Feldstein SN and Lange RA** (1999) Pliocene potassic magmas from the Kings River Region, Sierra Nevada, California: evidence for melting of a subduction modified mantle. *Journal of Petrology* **40**, 1301–20.
- Foley SF** (1992) Vein-plus-wall-rock melting mechanisms in the lithosphere and the origin of potassic alkaline magmas. *Lithos* **28**, 435–53.
- Foley SF, Venturelli G, Green DH and Toscani L** (1987) The ultrapotassic rocks: characteristics, classification, and constraints for petrogenetic models. *Earth-Science Reviews* **24**, 81–134.
- Foley SF, Yaxley GM, Rosenthal A, Buhre S, Kiseeva ES, Rapp RP and Jacob DE** (2009) The composition of near-solidus melts of peridotite in the presence of CO₂ and H₂O between 40 and 60 kbar. *Lithos* **112S**, 274–83.
- Hildebrand RS and Bowring SA** (1999) Crustal recycling by slab failure. *Geology* **27**, 11–14.
- Hou T, Zhang ZC, Keiding JK and Veksler IV** (2015) Petrogenesis of the ultrapotassic Fanshan intrusion in the North China Craton: implications for lithospheric mantle metasomatism and the origin of apatite ores. *Journal of Petrology* **56**, 893–918.
- Huang DL and Hou, QY** (2017) Devonian alkaline magmatism in the northern North China Craton: geochemistry, SHRIMP zircon U–Pb geochronology and Sr–Nd–Hf isotopes. *Geoscience Frontiers* **8**, 171–81.
- Ickert RB, Hiess J, Williams IS, Holden P, Ireland TR, Lanc P, Schram N, Foster JJ and Clement SW** (2008) Determining high precision, in situ, oxygen isotope ratios with a SHRIMP II: analyses of MPI-DING silicate-glass reference materials and zircon from contrasting granites. *Chemical Geology* **257**, 114–28.
- Jahn BM, Auvray B, Cornichet J, Bai YL, Shen QH and Liu DY** (1987) 3.5 Ga old amphibolites from eastern Hebei Province, China: field occurrence, petrography, Sm–Nd isochron age and REE geochemistry. *Precambrian Research* **34**, 311–46.
- Jamali H, Dilek Y, Daliran F, Yaghubpur A and Mehrabi B** (2010) Metallogeny and tectonic evolution of the Cenozoic Ahar–Arasbaran volcanic belt, northern Iran. *International Geology Review* **52**, 608–30. doi: [10.1080/00206810903416323](https://doi.org/10.1080/00206810903416323).
- Klimm K, Blundy JD and Green TH** (2008) Trace element partitioning and accessory phase saturation during H₂O-saturated melting of basalt with implications for subduction zone chemical fluxes. *Journal of Petrology* **49**, 523–53.
- Langmuir CH, Vocke RD, Jr, Hanson GN and Hart SR** (1978) A general mixing equation with applications to Icelandic basalts. *Earth and Planetary Science Letters* **37**, 380–92.
- Liu D, Zhao ZD, Zhu DC, Niu YL, Widom E, Teng FZ, DePaolo DJ, Ke S, Xu JF, Wang Q and Mo XX** (2015) Identifying mantle carbonatite metasomatism through Os–Sr–Mg isotopes in Tibetan ultrapotassic rocks. *Earth and Planetary Science Letters* **430**, 458–69.
- Liu DY, Nutman AP, Compston W, Wu JS and Shen QH** (1992) Remnants of ≥3800 Ma crust in the Chinese part of the Sino-Korean Craton. *Geology* **20**, 339–42.
- Liu YS, Gao S, Yuan HL, Zhou L, Liu, XM, Wang X, Hu ZC and Wang L** (2004) U–Pb zircon ages and Nd, Sr and Pb isotopes of lower crustal xenoliths from North China: insights on evolution of the lower continental crust. *Chemical Geology* **211**, 87–109.
- Ludwig KR** (2001) *Squid 1.02: A User's Manual*. Berkeley, California: Berkeley Geochronology Center, Special Publication No. 2, 19 pp.
- Ludwig KR** (2003) *User's Manual for Isoplot 3.00, a Geochronological Toolkit for Microsoft Excel*. Berkeley, California: Berkeley Geochronology Center, 70 pp.
- Mallik A, Nelson J and Dasgupta R** (2015) Partial melting of fertile peridotite fluxed by hydrous rhyolitic melt at 2–3 GPa: implications for mantle wedge hybridization by sediment melt and generation of ultrapotassic magmas in convergent margins. *Contributions to Mineralogy and Petrology* **169**, 48. doi: [10.1007/s00410-015-1139-2](https://doi.org/10.1007/s00410-015-1139-2).
- Martindale M, Skora S, Pickles J, Elliott T, Blundy J and Avanzinelli R** (2013) High pressure phase relations of subducted volcanoclastic sediments from the West Pacific and their implications for the geochemistry of Mariana arc magmas. *Chemical Geology* **342**, 94–109.
- McDonough WF** (1990) Constraints on the composition of the continental lithospheric mantle. *Earth and Planetary Science Letters* **101**, 1–18.
- Miller C, Schuster R, Klötzli U, Frank W and Purtscheller F** (1999) Post-collisional potassic and ultrapotassic magmatism in SW Tibet: geochemical and Sr–Nd–Pb–O isotopic constrains for mantle source characteristics and petrogenesis. *Journal of Petrology* **40**, 1399–1424.

- Nelson DR (1992) Isotopic characteristics of potassic rocks: evidence for the involvement of subducted sediments in magma genesis. *Lithos* **28**, 403–20.
- Niu XL, Chen B, Feng GY, Liu F and Yang JS (2017) Origin of Lamprophyres from the northern margin of the North China Craton: implications for mantle metasomatism. *Journal of the Geological Society* **174**, 353–64.
- Niu XL, Chen B, Liu AK, Suzuki K and Ma X (2012) Petrological and Sr-Nd-Os isotopic constraints on the origin of the Fanshan ultrapotassic complex from the North China Craton. *Lithos* **149**, 146–58.
- Niu XL, Yang JS, Liu F, Zhang HY and Yang MC (2016) Origin of Baotoudong syenites in North China Craton: petrological, mineralogical and geochemical evidence. *Science China – Earth Science* **59**, 95–110.
- Pearce JA and Peate DW (1995) Tectonic implications of the composition of volcanic arc magmas. *Annual Review of Earth and Planetary Sciences* **23**, 251–85.
- Plank T and Langmuir CH (1998) The chemical composition of subducting sediment and its consequences for the crust and mantle. *Chemical Geology* **145**, 325–94.
- Prelević D, Foley SF and Cvetković V (2012) A review of petrogenesis of Mediterranean Tertiary lamproites: a perspective from the Serbian ultrapotassic province. In *Cenozoic Volcanism in the Mediterranean Area* (eds L. Beccaluva, G. Bianchini and M. Wilson), pp. 113–29. Boulder, Colorado: Geological Society of America Special Paper 418.
- Prelević D, Foley SF, Romer R and Conticelli S (2008) Mediterranean Tertiary lamproites derived from multiple source components in postcollisional geodynamics. *Geochimica et Cosmochimica Acta* **72**, 2125–56.
- Pysklywec RN, Beaumont C and Fullsack P (2002) Lithospheric deformation during the early stages of continental collision: numerical experiments and comparison with South Island, New Zealand. *Journal of Geophysical Research: Solid Earth* **107**. <https://doi.org/10.1029/2001JB000252>.
- Rudnick RL and Gao S (2003) Composition of the continental crust. In *Treatise on Geochemistry*, vol. 3 (eds HD Holland and KK Turekian), pp. 1–64. Oxford: Elsevier-Perгамon.
- Rudnick RL, Gao S, Ling WL, Liu YS and McDonough WF (2004) Petrology and geochemistry of spinel peridotite xenoliths from Hannuoba and Qixia, North China craton. *Lithos* **77**, 609–37.
- Schellart WP, Stegman DR, Farrington RJ, Freeman J and Moresi L (2010) Cenozoic tectonics of western North America controlled by evolving width of Farallon slab. *Science* **329**, 316–19.
- Sekine T and Wyllie PJ (1983). Experimental simulation of mantle hybridization in subduction zones. *Journal of Geology* **91**, 511–28.
- Shaffer M, Hacker BR, Ratschbacher L and Kylander-Clark ARC (2017) Foundering triggered by the collision of India and Asia captured in xenoliths. *Tectonics* **36**, 1913–33. doi: [10.1002/2017TC004704](https://doi.org/10.1002/2017TC004704).
- Skora S and Blundy J (2010) High pressure hydrous phase relations of radiolarian clay and implication for the involvement of subducting sediment in arc magmatism. *Journal of Petrology* **51**, 2211–43.
- Song S, Wang MM, Xu X, Wang C, Niu Y, Allen MB and Su L (2015) Ophiolites in the Xing'an-Inner Mongolia accretionary belt of the CAOB: implications for two cycles of seafloor spreading and accretionary orogenic events. *Tectonics* **34**, 2221–48.
- Sun SS and McDonough WF (1989) Chemical and isotopic systematics of oceanic basalts: implications for mantle composition and processes. In *Magmatism in the Ocean Basins* (eds AD Saunders and MJ Norry), pp. 313–45. Geological Society of London, Special Publication no. 42.
- Tommasini S, Avanzinelli R and Conticelli S (2011) The Th/La and Sm/La conundrum of the Tethyan realm lamproites. *Earth and Planetary Science Letters* **301**, 469–78.
- Valley JW, Lackey JS, Cavosie AJ, Clechenko CC, Spicuzza MJ, Basei MAS, Bindeman IN, Ferreira VP, Sial AN, King EM, Peck WH, Sinha AK and Wei CS (2005) 4.4 billion years of crustal maturation: oxygen isotope ratios of magmatic zircon. *Contributions to Mineralogy and Petrology* **150**, 561–80.
- Wang K, Plank T, Walker JD and Smith EI (2002) A mantle melting profile across the basin and range, SW USA. *Journal of Geophysical Research* **107**. doi: [10.1029/2001JB0002092](https://doi.org/10.1029/2001JB0002092).
- Wang Y, Foley SF and Prelević D (2017) Potassium-rich magmatism from a phlogopite-free source. *Geology* **45**, 467–70.
- Wang Y, Zhou LY, Liu SF, Li JY and Yang TN (2018) Post-cratonization deformation processes and tectonic evolution of the North China Craton. *Earth-Science Reviews* **177**, 320–65.
- Wei CJ, Qian JH and Zhou XW (2014) Paleoproterozoic crustal evolution of the Hengshan–Wutai–Fuping region, North China Craton. *Geoscience Frontiers* **5**, 485–97.
- Wilhem C, Windley BF and Stampfli GM (2012) The Altaids of Central Asia: a tectonic and evolutionary innovative review. *Earth-Science Reviews* **113**, 303–41.
- Williams HM, Turner SP, Pearce JA, Kelley SP and Harris NBW (2004) Nature of the source regions for post-collisional, potassic magmatism in southern and northern Tibet from geochemical variations and inverse trace element modelling. *Journal of Petrology* **45**, 555–607.
- Williams IS (1998) U–Th–Pb geochronology by ion microprobe, applications of microanalytical techniques to understanding mineralizing processes. In *Reviews in Economic Geology*, vol. 7: Application of Microanalytical Techniques to Understanding Mineralizing Processes (eds MA McKibben, WC Shanks and WI Ridley), pp. 1–35. Littleton, Colorado: Society of Economic Geologists.
- Windley BF, Alexeev D, Xiao WJ, Kröner A and Badarch G (2007) Tectonic models for accretion of the Central Asian Orogenic Belt. *Journal of the Geological Society* **164**, 31–47.
- Wu FY, Lin JQ, Wilde SA, Zhang, XO and Yang, JH (2005) Nature and significance of the Early Cretaceous giant igneous event in eastern China. *Earth and Planetary Science Letters* **233**, 103–19.
- Xiao WJ, Windley B, Hao J and Zhai MG (2003) Accretion leading to collision and the Permian Solonker suture, Inner Mongolia, China: termination of the Central Asian Orogenic Belt. *Tectonics* **22**, 1069–89.
- Yan GH, Mu, BL, Xu, BL, He, GQ, Tan, LK, Zhao, H, He, ZF, Zhang, RH and Qiao, GS (1999) Triassic alkaline intrusions in the Yanliao-Yinshan area: their chronology, Sr, Nd and Pb isotopic characteristics and their implications. *Science China – Earth Science* **42**, 582–7.
- Yang JH, Sun JF, Zhang M, Wu FY and Wilde SA (2012) Petrogenesis of silica-saturated and silica-undersaturated syenites in the northern North China Craton related to post-collisional and intraplate extension. *Chemical Geology* **328**, 149–67.
- Zhang GH, Zhou XH, Sun M, Chen SH and Feng JL (1998) Sr, Nd and Pb isotopic characteristics of granulite and pyroxenite xenoliths in Hannuoba basalts, Hebei Province, and their implications for geological processes. *Acta Petrologica Sinica* **14**, 190–7 (in Chinese with English abstract).
- Zhang QQ, Zhang, SH, Zhao Y and Liu JM (2018) Devonian alkaline magmatic belt along the northern margin of the North China Block: petrogenesis and tectonic implications. *Lithos* **302–303**, 496–518.
- Zhang SH, Zhao Y, Kröner A, Liu XM, Xie LW and Chen FK (2009) Early Permian plutons from the northern North China Block: constraints on continental arc evolution and convergent margin magmatism related to the Central Asian Orogenic Belt. *International Journal of Earth Science* **98**, 1441–67.
- Zhang SH, Zhao Y, Ye H, Liu J-M and Hu Z-C (2014) Origin and evolution of the Bainaimiao arc belt: implications for crustal growth in the southern Central Asian orogenic belt. *Geological Society of America Bulletin* **126**, 1275–1300.
- Zhang SH, Zhao Y, Ye H, Hou KJ and Li CF (2012) Early Mesozoic alkaline complexes in the northern North China Craton: implications for cratonic lithospheric destruction. *Lithos* **155**, 1–18.
- Zhang XH, Zhang, HF, Jiang N, Zhai MG and Zhang, YB (2010) Early Devonian alkaline intrusive complex from the northern North China craton: a petrological monitor of post-collisional tectonics. *Journal of the Geological Society* **167**, 717–30.
- Zhang ZQ, Wu JS and Ye XJ (1991) Archean metamorphic rocks from the lower Fuping Group in the Mt. Taihang region, North China: REE geochemistry, Rb–Sr, and Sm–Nd ages and implications. *Geochimica* **2**, 118–27 (in Chinese with English abstract).
- Zhao GC (2001) Palaeoproterozoic assembly of the North China Craton. *Geological Magazine* **138**, 87–91.
- Zhao GC and Zhai MG (2013) Lithotectonic elements of Precambrian basement in the North China Craton: review and tectonic implications. *Gondwana Research* **23**, 1207–40.
- Zhao Z, Mo X, Dilek Y, Niu Y, DePaolo DJ, Robinson P, Zhu D, Sun C, Dong G, Zhou S, Luo Z and Hou Z (2009) Geochemical and Sr-Nd-Pb-O

- isotopic compositions of the post-collisional ultrapotassic magmatism in SW Tibet: petrogenesis and implications for India intra-continental subduction beneath southern Tibet. *Lithos* **113**, 190–212.
- Zheng JP and Lu FX** (1999) Mantle xenoliths from kimberlites, Shandong and Liaoning: Paleozoic mantle character and its heterogeneity. *Acta Petrologica Sinica* **15**, 65–74 (in Chinese with English abstract).
- Zhou XH, Sun M, Zhang GH and Chen SH** (2002) Continental crust and lithospheric mantle interaction beneath North China: isotopic evidence from granulite xenoliths in Hannuoba, Sino-Korean craton. *Lithos* **62**, 111–24.
- Zhu RX, Yang JH and Wu FY** (2012) Timing of destruction of the North China Craton. *Lithos* **149**, 51–60.